



The Detectability and Characterization of the TRAPPIST-1 Exoplanet Atmospheres with JWST

Jacob Lustig-Yaeger^{1,2} , Victoria S. Meadows^{1,2} , and Andrew P. Lincowski^{1,2}

¹ Department of Astronomy and Astrobiology Program, University of Washington, Box 351580, Seattle, Washington 98195, USA; jlustig@uw.edu

² NASA NExSS Virtual Planetary Laboratory, Box 351580, University of Washington, Seattle, Washington 98195, USA

Received 2019 March 26; revised 2019 May 10; accepted 2019 May 14; published 2019 June 21

Abstract

The *James Webb Space Telescope (JWST)* will offer the first opportunity to characterize terrestrial exoplanets with sufficient precision to identify high mean molecular weight atmospheres, and TRAPPIST-1's seven known transiting Earth-sized planets are particularly favorable targets. To assist community preparations for *JWST* observations, we use simulations of plausible post-ocean-loss and habitable environments for the TRAPPIST-1 exoplanets, and test simulations of all bright object time-series spectroscopy modes and all Mid-Infrared Instrument photometry filters to determine optimal observing strategies for atmospheric detection and characterization using both transmission and emission observations. We find that transmission spectroscopy with the Near-Infrared Spectrograph Prism is optimal for detecting terrestrial, CO₂-containing atmospheres, potentially in fewer than 10 transits for all seven TRAPPIST-1 planets, if they lack high-altitude aerosols. If the TRAPPIST-1 planets possess Venus-like H₂SO₄ aerosols, up to 12 times more transits may be required to detect an atmosphere. We present optimal instruments and observing modes for the detection of individual molecular species in a given terrestrial atmosphere and an observational strategy for discriminating between evolutionary states. We find that water may be prohibitively difficult to detect in both Venus-like and habitable atmospheres, due to its presence lower in the atmosphere where transmission spectra are less sensitive. Although the presence of biogenic O₂ and O₃ will be extremely challenging to detect, abiotically produced oxygen from past ocean loss may be detectable for all seven TRAPPIST-1 planets via O₂-O₂ collisionally induced absorption at 1.06 and 1.27 μm, or via NIR O₃ features for the outer three planets. Our results constitute a suite of hypotheses on the nature and detectability of highly evolved terrestrial exoplanet atmospheres that may be tested with *JWST*.

Key words: planets and satellites: atmospheres – planets and satellites: individual (TRAPPIST-1) – planets and satellites: terrestrial planets – techniques: spectroscopic

1. Introduction

The discovery of Earth-sized planets in temperate orbits around nearby, low-mass stars opens a new door into the era of terrestrial exoplanet atmospheric characterization (Berta-Thompson et al. 2015; Anglada-Escudé et al. 2016; Gillon et al. 2016, 2017; Dittmann et al. 2017; Luger et al. 2017b). Transmission and emission (secondary eclipse) spectroscopy of transiting rocky worlds with the upcoming *James Webb Space Telescope (JWST)* may offer a first glimpse into the atmospheres of terrestrial exoplanets (Morley et al. 2017; Kalirai 2018) and a first opportunity to search for signs of habitability (Lincowski et al. 2018) and biosignatures beyond the solar system (Cowan et al. 2015).

The TRAPPIST-1 system of seven transiting Earth-sized exoplanets (Gillon et al. 2016, 2017; Luger et al. 2017b) is observationally favorable for the atmospheric characterization of small exoplanets. TRAPPIST-1 is a late M dwarf (M8V; Liebert & Gizis 2006) with a small radius ($0.121 R_{\odot}$; Van Grootel et al. 2018), which increases planetary transit and eclipse depths; it has a low effective temperature (2511 K; Van Grootel et al. 2018), which increases the eclipse depth; and it is near Earth (12.2 pc; Gillon et al. 2016). These system properties increase sensitivity to atmospheric spectral features

in transmission and emission spectroscopy, particularly for small, temperate planets.

Observations of the TRAPPIST-1 planets with the *Kepler*, *Hubble (HST)*, and *Spitzer* space telescopes suggest that the innermost six planets do not have primordial, low mean molecular weight atmospheres, but whether they have high molecular weight atmospheres or no atmospheres at all requires observations with future facilities. *HST* Wide Field Camera 3 transmission spectroscopy has ruled out H₂-dominated atmospheres for most of the TRAPPIST-1 planets (de Wit et al. 2016, 2018), and instead they may have secondary outgassed atmospheres composed of relatively high mean molecular weight gases (Moran et al. 2018). Secondary atmospheres are more difficult to detect—or rule out—than primordial atmospheres, and they may span a large range in temperature, pressure, and composition. Consequently, a broad variety of potential atmospheres are consistent with the current modest observational constraints (Delrez et al. 2018; Lincowski et al. 2018).

Alternatively, the planets could have no atmospheres, although outgassing from the possibly high-volatile-content interiors of the TRAPPIST-1 planets may make that outcome less likely. Simulations suggest that the TRAPPIST-1 planets could have had their atmospheres completely stripped (e.g., Airapetian et al. 2017; Roettenbacher & Kane 2017; Dong et al. 2018), although some models of M dwarf planets suggest that atmospheric loss rates may be less than the replenishment rate via outgassing from a planetary interior (Bolmont et al. 2017; Garcia-Sage et al. 2017), such that atmospheres may be



Original content from this work may be used under the terms of the [Creative Commons Attribution 3.0 licence](#). Any further distribution of this work must maintain attribution to the author(s) and the title of the work, journal citation and DOI.

retained. The TRAPPIST-1 planets may also have larger volatile reservoirs than solar system terrestrials. Masses derived from transit timing variation analyses of *Kepler* (Grimm et al. 2018) and *Spitzer* observations (Delrez et al. 2018) suggest that the planets have densities between 0.6 and 1.0 ρ_{\oplus} , consistent with a rocky composition with a significant fraction of ices (Grimm et al. 2018). This conclusion is supported by the resonant chain structure of the TRAPPIST-1 system, which suggests inward migration from more volatile-rich formation orbits (Luger et al. 2017b). Determining whether the interplay of planetary processes over time will allow M dwarf terrestrial planets to maintain high molecular weight atmospheres and support habitability will be key science questions for *JWST*.

Previous simulations have demonstrated the plausibility of detecting terrestrial atmospheres with *JWST* for M dwarf planetary systems in general (e.g., Belu et al. 2011; Barstow et al. 2016), and for the TRAPPIST-1 planets in particular (Barstow & Irwin 2016; Morley et al. 2017; Batalha et al. 2018; Krissansen-Totton et al. 2018). Morley et al. (2017) considered Venus-like, Earth-like, and Titan-like atmospheres in thermochemical equilibrium and found that CO₂-dominated atmospheres could be detected for six of the seven TRAPPIST-1 planets in fewer than 20 transits with *JWST* Near-Infrared Spectrograph (NIRSpec)/G235M, and secondary eclipse photometry with *JWST*/Mid-Infrared Instrument (MIRI) could readily detect thermal emission from TRAPPIST-1b and c, and possibly d, e, and f. Batalha et al. (2018) investigated optimal strategies for *JWST* observations of the TRAPPIST-1 system and found that allowing NIRSpec Prism to slightly saturate at the peak of the stellar spectral energy distribution (SED) could allow the dominant absorber to be detected in 10 transits of H₂O-, CO₂-, and N₂-dominated atmospheres. Krissansen-Totton et al. (2018) investigated the potential detectability of anoxic biosignatures in the atmosphere of TRAPPIST-1e and concluded that 10 transits observed with *JWST* NIRSpec Prism may be sufficient to detect CO₂ and constrain the CH₄ abundance enough to rule out nonbiological CH₄ production. Recently, Wunderlich et al. (2019) considered the detectability of photochemically self-consistent Earth-like planets in the habitable zone of various M dwarf spectral types, including TRAPPIST-1, and found that H₂O, CH₄, and CO₂ may be detectable in \sim 10 transits with *JWST*. However, this study did not consider non-Earth-like planetary compositions, or the effect of clouds and hazes.

These previous simulations of TRAPPIST-1 planetary atmospheres did not include photochemical forcing by the late M dwarf SED on multiple plausible planetary environments, both habitable and uninhabitable. Photochemistry can have significant impacts on terrestrial atmospheric composition (Segura et al. 2005; Rugheimer et al. 2015) and haze formation (Arney et al. 2017, 2018), which can in turn modify the resultant temperature structure (Lincowski et al. 2018), impacting the predicted spectrum in both transmission and emission. Models that include photochemistry and haze formation for terrestrial atmospheres will better predict the atmospheric composition and inform the preparation and interpretation of upcoming observations with *JWST* (Lincowski et al. 2018).

In this paper, we explore the potential for *JWST* to detect and characterize the TRAPPIST-1 planetary atmospheres and distinguish between model predictions for evolutionary outcomes and different atmospheric states. As input, we use the

climatically and photochemically self-consistent atmospheric and spectral simulations of Lincowski et al. (2018), who used a rigorous line-by-line 1D radiative–convective–equilibrium climate model coupled with a 1D photochemical model to simulate different habitable and post-ocean-loss environments for the TRAPPIST-1 planets. The atmospheric bulk compositions considered by Lincowski et al. (2018) are motivated by the early high luminosity of late M dwarf stars (Baraffe et al. 2015) like TRAPPIST-1, which may drive early ocean loss and the generation of tens to thousands of bars of O₂ (Luger & Barnes 2015; Bolmont et al. 2017; Lincowski et al. 2018; Meadows et al. 2018; Wordsworth et al. 2018). The final inventory of O₂ may be severely reduced by atmospheric and surface-loss processes such that only a few bars of O₂ remain (Schaefer et al. 2016; Wordsworth et al. 2018). Depending on the initial water inventory, this process may have exhausted the entire planet’s water supply, leaving it desiccated, or the planet may have formed with enough water to endure such vigorous loss. For the ocean-loss planets with efficient O₂ sinks and ongoing outgassing of volatiles, large quantities of CO₂ may build up, forming a Venus-like atmosphere (Meadows et al. 2018). Lincowski et al. (2018) also considered a habitable ocean world for TRAPPIST-1e, for the scenario where it formed with an appreciable H₂ envelope, which was subsequently stripped to reveal a habitable core (Luger et al. 2015).

To understand the nature and possible habitability of terrestrial exoplanets, we will need a systematic approach to environmental assessment that starts with the most scientifically significant and least expensive observation, and builds from there. For terrestrial planets orbiting M dwarfs, the first property to be determined is whether or not they have an atmosphere. If an atmosphere can be confirmed, then subsequent studies will focus on determining the nature of that atmosphere, and whether there are atmospheric characteristics that could discriminate between evolutionary outcomes. Finally, a deeper dive to search for signs of habitability, including the presence of an ocean (see Lustig-Yaeger et al. 2018; Robinson 2018) and biosignatures (see Schwertner et al. 2018), may be warranted for planets whose initial characterization does not preclude habitable conditions.

Here we determine the feasibility of atmospheric characterization for the seven known TRAPPIST-1 exoplanets by first identifying optimal instrument selection and experiments to test whether or not the TRAPPIST-1 planets have atmospheres. We then determine how to best detect specific molecules as a second step of atmospheric characterization, and discriminate between different plausible climate and photochemically self-consistent atmospheres (e.g., O₂ dominated, CO₂ dominated; Lincowski et al. 2018) using *JWST* transmission and emission photometry and spectroscopy.

The different post-runaway, evolved planet atmospheres considered here are by no means a comprehensive set of evolutionary outcomes, but rather a representative subset of potential physically and chemically motivated atmospheres for which we can predict spectra. By understanding the detectability of spectral discriminants for the TRAPPIST-1 planets, we develop informed hypotheses on the nature of these planets that may later be tested with *JWST* observations.

The structure of the paper is as follows. In Section 2 we present the models and methods used to simulate *JWST* data and find the optimal *JWST* modes for detecting and characterizing plausible planet compositions. We describe our

results in Section 3, offer a discussion of the significance of those results in Section 4, and conclude in Section 5.

2. Methods

In the following subsections, we present our methods for assessing the detectability of different self-consistent atmospheric compositions for the seven TRAPPIST-1 planets with different instruments and observational modes available to *JWST*. We first describe the *JWST* noise models used in this work (Section 2.1), which include an MIRI photometry component and a spectroscopy component using PandExo (Batalha et al. 2017). We then detail our model inputs (Section 2.2) and outline a series of experiments that can be used to successively characterize terrestrial planet environments and determine optimal observing modes (Section 2.3).

2.1. JWST Noise Modeling

We simulate synthetic exoplanet time-series spectroscopy and photometry with *JWST* to consider observations during transit (transmission) and secondary eclipse (emission). In the following two subsections, we detail our modeling of *JWST*/MIRI photometry (Section 2.1.1) and *JWST* spectroscopy (Section 2.1.2).

2.1.1. JWST/MIRI Photometry

Filter photometry with *JWST*'s MIRI imager has been suggested to offer an efficient means of performing an initial characterization of Earth-sized planets around low-mass stars (Morley et al. 2017). To assess MIRI photometry, we develop a basic MIRI imaging noise model for exoplanet transit and secondary eclipse observations.

The number of photons from the planet incident upon the detector is

$$N_p = T_{\text{exp}} \frac{F_p T A \lambda \Delta \lambda}{hc}, \quad (1)$$

where T_{exp} is the exposure time, F_p is the spectral flux density (e.g., $\text{W m}^{-2} \mu\text{m}^{-1}$) from the planet, T is the filter throughput, A is the telescope collecting area (25 m^2), λ is wavelength, $\Delta \lambda$ is the width of the wavelength bin, h is Planck's constant, and c is the speed of light. Note that the exposure time used in our photometry model is discretized in terms of the simulated planet's transit duration, but does not explicitly depend on the MIRI integration times or number of groups per integration, as our time-series spectroscopy noise modeling with PandExo does. Photon conversion efficiency curves for the MIRI imager were acquired online³ (Glasse et al. 2015). Photons from the star are calculated analogously using Equation (1) by replacing the planet flux with the stellar flux.

The signal-to-noise (S/N) ratio on the transit depth is given by

$$\text{S/N}_T = \frac{N_s (R_p/R_s)^2}{\sqrt{(N_s + N_{bg})/n_{\text{out}} + N_{bg} + N_s [1 - (R_p/R_s)^2]}}, \quad (2)$$

where N_s is the number of photons from the star, N_{bg} is the number of photons from background sources, and n_{out} is the number of out-of-transit transit durations observed. Background

photon noise is calculated using the seven-component graybody model of Glasse et al. (2015), which includes telescope thermal and scattered zodiacal noise contributions. The S/N on the photons detected from a planet observed in secondary eclipse is given by

$$\text{S/N}_E = \frac{N_p}{\sqrt{(N_p + N_s + N_{bg})/n_{\text{out}} + N_s + N_{bg}}}, \quad (3)$$

where N_p is the number of photons from the planet. Derivations of Equations (2) and (3) are provided in Appendix A.

Saturation must be considered when planning long exposures necessary to characterize small exoplanets around nearby stars. Using the bright source limits of Glasse et al. (2015), we find that TRAPPIST-1 will saturate MIRI in the two shortest wavelength filters, F560W and F770W, for the shortest exposures allowed in the standard imaging mode. Although these shorter wavelength filters may saturate, we nonetheless consider MIRI photometry in all nine filters (F560W, F770W, F1000W, F1130W, F1280W, F1500W, F1800W, F2100W, and F2550W) to assess the atmospheric information contained in each.

2.1.2. JWST Spectroscopy

We use the *JWST* time-series spectroscopy simulator PandExo⁴ (version 1.1.2; Batalha et al. 2017, 2018) to model different observing modes and their associated noise sources for transmission and emission spectroscopy. PandExo leverages the core of the Space Telescope Science Institute's Exposure Time Calculator, Pandeia⁵ (version 1.2.2; Pontoppidan et al. 2016), to calculate 3D data cubes for realistic PSF modeling. We refer the reader to Batalha et al. (2017) for a thorough description of the model and its benchmarking.

We consider a broad variety of *JWST* instruments and modes that are capable of exoplanet transmission and emission spectroscopy and available using PandExo. We include the Near-Infrared Camera (NIRCam; Greene et al. 2007, 2017) using the grism time-series mode, NIRSpec (Bagnasco et al. 2007; Ferruit et al. 2014), the Near Infrared Imager and Slitless Spectrograph (NIRISS; Doyon et al. 2012) using the single-object slitless spectroscopy (SOSS) mode, and the MIRI (Bouchet et al. 2015) low-resolution spectrometer (LRS; Kendrew et al. 2015).

Table 1 summarizes the different *JWST* instruments and modes used to simulate transmission and emission spectroscopy of the TRAPPIST-1 system. Specifically, Table 1 lists the instrument, mode, disperser, filter, subarray, read mode, wavelength range, and nominal spectral resolving power used in our PandExo calculations. Table 1 also presents the number of groups per integration, the observing efficiency, and the number of saturated pixels at the end of the ramp for our simulated observations of the TRAPPIST-1 system with each instrument. We use NIRSpec Prism in three configurations. First, we use the SUB512 subarray (frame time: 0.226 s) with two groups per integration set by PandExo to avoid pixel saturation. Second, we use the SUB512s subarray (frame time: 0.144 s) with three groups per integration, again set by PandExo. Finally, we simulate a partial saturation strategy by using the SUB512 and SUB512s subarrays with six groups per

³ <http://ircamera.as.arizona.edu/MIRI/pces.htm>

⁴ <https://natashabatalha.github.io/PandExo/>

⁵ <https://jwst.etc.stsci.edu/>

Table 1
JWST Instruments Used in This Study and The Observability of TRAPPIST-1 with Them

Instrument	Mode	Disperser	Filter	Subarray	Read Mode	λ (μm)	R ($\lambda/\Delta\lambda$)	N_{groups}	Efficiency	N_{sat}
NIRCam	ssgrism	grism R	f322w2	subgrism64	rapid	2.42–4.15	~1600	303	99.34%	0
NIRCam	ssgrism	grism R	f444w	subgrism64	rapid	3.70–5.00	~1600	342	99.42%	0
NIRISS	SOSS	gr700xd	None	substrip96	nirapid	0.6–2.8	~700	52	96.23%	0
NIRISS	SOSS	gr700xd	None	substrip256	nirapid	0.6–2.8	~700	21	90.91%	0
NIRSpec	fixed slit	g140h	f100lp	sub2048	nrsrapid	0.97–1.82	~2700	39	95.00%	0
NIRSpec	fixed slit	g140m	f100lp	sub2048	nrsrapid	0.97–1.84	~1000	14	86.67%	0
NIRSpec	fixed slit	g235h	f170lp	sub2048	nrsrapid	1.66–3.05	~2700	41	95.24%	0
NIRSpec	fixed slit	g235m	f170lp	sub2048	nrsrapid	1.66–3.07	~1000	14	86.67%	0
NIRSpec	fixed slit	g395h	f290lp	sub2048	nrsrapid	2.87–5.14	~2700	82	97.59%	0
NIRSpec	fixed slit	g395m	f290lp	sub2048	nrsrapid	2.87–5.10	~1000	29	93.33%	0
NIRSpec	fixed slit	prism	clear	sub512	nrsrapid	0.6–5.3	~100	2	33.33%	0
NIRSpec	fixed slit	prism	clear	sub512s	nrsrapid	0.6–5.4	~100	3	50.00%	0
NIRSpec	fixed slit	prism	clear	sub512	nrsrapid	0.6–5.5	~100	6	71.43%	47
NIRSpec	fixed slit	prism	clear	sub512s	nrsrapid	0.6–5.6	~100	6	71.43%	19
MIRI	LRS	p750l	None	slitlessprism	fast	0.5–12.0	~100	139	98.57%	0

Note. N_{groups} is the number of groups per integration and N_{sat} is the number of saturated pixels at the end of the ramp. The right three columns are outputs from the PandExo *JWST* noise model specifically for observations of the TRAPPIST-1 system. We refer to the partially saturated NIRSpec Prism sub512 configuration with $N_{\text{groups}} = 6$ as “NIRSpec Prism*.”

integration to allow for slight pixel saturation near the peak of the SED (Batalha et al. 2018). This modification improves the duty cycle from 33.3% (50%) to 71.4% for the SUB512 (SUB512s) subarray, as shown in Table 1 (see “Efficiency” column). We refer to this partially saturated NIRSpec Prism mode as “NIRSpec Prism*” hereafter.

2.2. Noise Model Inputs

For the stellar input to the PandExo noise model, we approximate the TRAPPIST-1 stellar spectrum, which has yet to be observed, using a PHOENIX stellar model (Husser et al. 2013) with an effective temperature of $T = 2511$ K, metallicity of $[\text{Fe}/\text{H}] = 0.04$, and surface gravity $\log g = 5.23$ (Delrez et al. 2018), normalized to the K -band magnitude of TRAPPIST-1 ($K = 10.30$; Grimm et al. 2018). However, we ignore the effects of stellar opacity in the MIR, stellar variability due to rotation and flaring during periods of observation (Vida et al. 2017; Morris et al. 2018), and heterogeneous stellar photospheres (Rackham et al. 2018; Zhang et al. 2018).

We use the modeled transmission and emission spectra of Lincowski et al. (2018) as inputs into the noise models to assess the detectability of photochemically and climatically self-consistent TRAPPIST-1 planet’s atmospheres. The climate model developed by Robinson & Crisp (2018) and Lincowski et al. (2018) uses line-by-line radiative transfer computed by the Spectral Mapping and Atmospheric Radiative Transfer (SMART) code (Meadows & Crisp 1996, developed by D. Crisp), and can generate top-of-atmosphere planetary radiances and transmission spectra (Robinson 2017) of its equilibrium climate and photochemical states. See Lincowski et al. (2018) for a thorough description of the climate and photochemical modeling, and subsequent climate results. Note that we refer to the (1 bar) habitable “aqua planet” atmosphere from Lincowski et al. (2018) as the “1 bar H_2O ” atmosphere in this paper. The stellar spectrum used in the optical through the MIR in Lincowski et al. (2018) is identical to the stellar spectrum used here for the *JWST* noise model input.

For target exposure times per transit, we use the median transit durations for the TRAPPIST-1 planets from Grimm et al. (2018), and for photometry and spectroscopy noise calculations, we assume that an equal amount of time is spent observing in transit/eclipse versus out of transit/eclipse. For PandExo, we assume saturation to be an exposure level 80% of the full well, and we impose no strict noise floor for *JWST* spectroscopy (see Greene et al. 2016). We compute noise calculations across a grid in the number of transits/eclipses ([1, 100]), and then use these results to derive and report the number of transits/eclipses needed to meet specific atmospheric detection and characterization metrics, as described in the following section.

2.3. Observing Experiments

We aim to identify the optimal observing approaches for *JWST* to (1) detect the presence of the TRAPPIST-1 planet atmospheres, and (2) to characterize the composition of the atmospheres, assuming the TRAPPIST-1 planets possess atmospheres similar in nature to the evolved atmospheres modeled in Lincowski et al. (2018). We consider an atmosphere to be detected when sufficient S/N is achieved on any spectral feature in a transmission or emission spectrum. For atmospheric characterization, we consider a specific molecule in the atmosphere to be detected when sufficient S/N is attained on the contribution to the spectrum from that molecule, which may include multiple bands from a given molecule. Next, we detail our S/N approach for ruling out a fiducial spectrum, and then describe how the method is used to quantify the detectability of atmospheres and specific molecules within them.

2.3.1. S/N Approach

We now define an S/N approach to determine the confidence with which we can rule out that our data match a fiducial transmission or emission spectrum—which is a featureless spectrum for the case of detecting atmospheres.

For each atmospheric model and *JWST* instrument considered, we employ the following procedure for both transit and secondary eclipse geometries. First, we run the PandExo

JWST noise model across a grid in number of transits/eclipses (n_{occ}) from 1 to 100, which is sufficient to establish a simple S/N scaling relationship. Second, we determine the S/N on the difference between the model spectrum and the fiducial spectrum, and calculate the total expected $\langle \text{S/N} \rangle$ (defined below) by summing this difference over wavelength. Finally, we solve for number of transits/eclipses, n_{occ} , such that a given $\langle \text{S/N} \rangle$ is achieved.

We define the total expected S/N using a $\Delta\chi^2$ test formalism, which is common for model selection applications. For many random drawings of synthetic data with Gaussian noise, the expected value for $\Delta\chi^2$ between two models (m_1 and m_2) is simply

$$\langle \Delta\chi^2 \rangle = \sum_{i=1}^{N_\lambda} \left(\frac{m_{1,i} - m_{2,i}}{\sigma_i} \right)^2, \quad (4)$$

assuming that the observations with uncertainties σ are truly sampled from one of the models (m_1 in this case), and where the sum is over all N_λ spectral elements for a particular instrument. Gaussian noise is not added to the synthetic spectra both to speed up the calculation of the mean result and to avoid any single random data realization from biasing our results (e.g., Feng et al. 2018). The numerator in the sum in Equation (4) is the “signal” used to discriminate between the two models, while the denominator is the “noise” on the observations. For convenience, we define

$$\text{S/N}_i = \frac{m_{1,i} - m_{2,i}}{\sigma_i}, \quad (5)$$

which is the individual S/N contribution from each spectral element to model m_2 being ruled out in favor of model m_1 . Equation (4) may then be rewritten in terms of S/N_i and what we refer to as the total expected S/N,

$$\langle \text{S/N} \rangle = \sqrt{\langle \Delta\chi^2 \rangle} = \sqrt{\sum_{i=1}^{N_\lambda} (\text{S/N}_i)^2}. \quad (6)$$

Equation (6) is particularly useful because the quadrature sum over wavelength allows for the comparison between multiple different *JWST* instruments that may have different spectral resolutions and wavelength ranges, and for a comparison between transmission and emission spectroscopy for the same hypothesis (e.g., the planet does not have an atmosphere).

We caution that Equation (6) is equal to the confidence in the detection of model m_1 in units of standard deviations (number of “sigma” n_σ), only in the case where each model has one degree of freedom. To avoid assumptions on the degrees of freedom and degeneracies associated with spectral models, we simply report $\langle \text{S/N} \rangle$ with the understanding that these are upper limits on the confidence in the detection. Furthermore, when we report the number of transits/eclipses to rule out the fiducial model to a given $\langle \text{S/N} \rangle$, these are lower limits; additional sources of uncertainty and/or retrieval model complexity may require that more transits/eclipses be observed.

We now detail the fiducial spectral models that are used to detect the presence of an atmosphere and the individual molecules within it.

2.3.2. Detecting the Presence of an Atmosphere

The spectra of planets with atmospheres can be discriminated from the featureless spectra of airless worlds by the presence of spectral absorption features. This approach works best for atmospheres with strong absorption features, but will be challenging for transmission spectroscopy if molecular absorption is suppressed by a high mean molecular weight atmosphere (Miller-Ricci et al. 2009), the presence of clouds and hazes (Berta et al. 2012; Ehrenreich et al. 2014; Knutson et al. 2014; Kreidberg et al. 2014; Nikolov et al. 2015), or atmospheric refraction (Bétrémiéieux & Kaltenegger 2014; Misra et al. 2014). In these cases, higher S/N observations will be required to detect the presence of an atmosphere. Here we assess the detectability of realistic terrestrial atmospheres with clouds and hazes in transmission by comparing their spectra to a baseline featureless spectrum that is modeled as the best-fitting constant planet radius with wavelength. For the corresponding emission spectrum test, we model the featureless spectrum as the ratio of two blackbodies at the stellar effective temperature and best-fitting planetary equilibrium temperature (set by a variable bond albedo).

While there are several “false negative” processes that could suppress the signal from an atmosphere as described above, one “false positive” process is worth considering: the possibility that surface mineralogy could produce wavelength-dependent features in emission spectra of airless worlds. However, as we will show, these features are unlikely to be as prominent as atmospheric features, and this is especially true in realistic cases where multiple reflections occur within the mineral surface. Specifically, by Kirchoff’s law of thermal radiation, the emissivity ϵ is related to the reflectance R by (Nicodemus 1965)

$$\epsilon = 1 - R. \quad (7)$$

The emissivity then regulates the efficiency of thermally radiated flux F_λ relative to a perfect blackbody $B_\lambda(T)$ via

$$F_\lambda = \epsilon B_\lambda(T), \quad (8)$$

for an object with an equilibrium temperature T . However, Equation (8) uses the effective emissivity,

$$\epsilon_e = 1 - (1 - \epsilon)^{(n+1)}, \quad (9)$$

which accounts for the number of reflections n within the material, and ultimately decreases the contrast of mineralogical features in the thermal emission spectrum (Kirkland et al. 2003; Hu et al. 2012).

Figure 1 compares secondary eclipse spectrum models for different assumed end-member planet mineralogical compositions. Emission spectra are shown for planets at the zero bond albedo equilibrium temperature of TRAPPIST-1b composed solely of quartz, basalt, olivine, pyroxene, hematite, anorthite, enstatite, saponite, and feldspar—a selection of common rocks and minerals found in terrestrial solar system bodies. For comparison, also shown are emission spectra with strong atmospheric absorption features from the climatically and photochemically self-consistent 100 bar O₂-dominated and 92 bar CO₂-dominated atmospheres from Lincowski et al. (2018).

In some cases, mineralogical surface emission features are comparable in signal contrast to model atmospheric thermal emission features, but under most plausible physical scenarios, an airless rock would likely have significantly lower spectral variation than atmospheric features. The single-reflection

TRAPPIST-1b : Airless Rocks in Eclipse

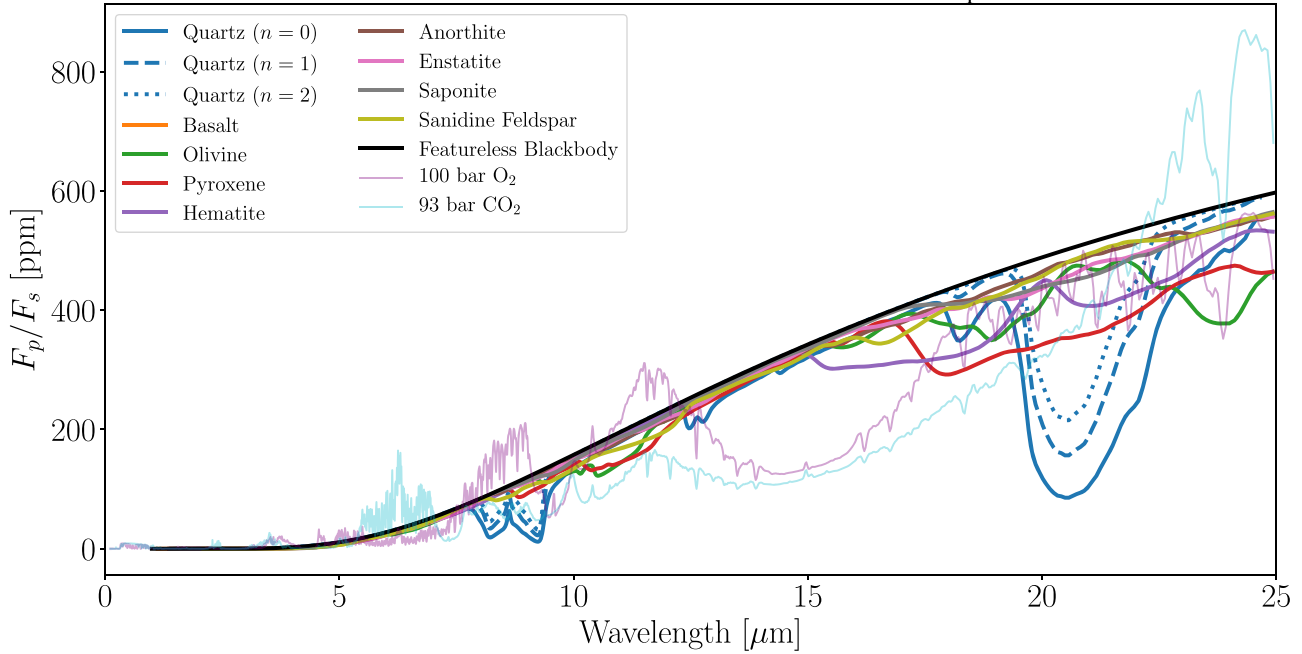


Figure 1. Secondary eclipse spectrum models of TRAPPIST-1b assuming different end-member planet mineralogical compositions. The black line shows a featureless blackbody curve, corresponding to the zero bond albedo planet equilibrium temperature, from which all of the thermal emission curves from rock-forming minerals (thick color lines) deviate due to non-unity, wavelength-dependent emissivities. The three line styles for the quartz curves demonstrate the reduction in effective emissivity due to n reflections within the rock (see Equation (9)). The thin purple and teal lines show the expected emission spectrum for TRAPPIST-1b if it were to possess a climatically and photochemically self-consistent thick O_2 - or a CO_2 -dominated atmosphere, respectively (Lincowski et al. 2018).

quartz silicate features between $\sim 8\text{--}10 \mu\text{m}$ and $\sim 19\text{--}23 \mu\text{m}$ are strong and rival the strength of the atmospheric features caused by O_3 , CO_2 , and H_2O over this wavelength range. However, single reflections are unlikely, and both multiple reflections and blends of different minerals would decrease the contrasts on features from any one of the representative end-member cases, producing a relatively featureless thermal emission spectrum.

Throughout the rest of the paper, unless otherwise stated, we adopt the assumption that detecting deviations from blackbody emission in a secondary eclipse spectrum is evidence of an atmosphere. However, in Section 3 we further explore the detectability of quartz silicate emissivity features in the emission spectrum of TRAPPIST-1b observed with MIRI LRS as an optimistic limiting case on the potential signal from an airless body.

Figures 2 and 3 provide a specific example of a test for the presence of a 10 bar CO_2 atmosphere, using both transmission (with NIRSPEC Prism*) and emission (with MIRI LRS) spectroscopy, respectively. The bottom panel of each figure shows a direct comparison between the template spectrum and the featureless model that best fits the template spectrum. The color contours show the magnitude of difference between the two spectra in the bottom panel divided by the noise (S/N_0) as a function of wavelength and number of occultations. The right panels show the total expected S/N , $\langle \text{S}/\text{N} \rangle$, as a function of number of occultations, which is the total signal of the atmosphere over the wavelength range of the instrument. The quadrature sum over wavelength not only allows for a comparison between different instruments that naturally accounts for the native resolution of and noise incurred by the instrument, but also a comparison between transmission and emission spectroscopy. Comparing Figures 2 and 3, we see

that if TRAPPIST-1b possesses a 10 bar high CO_2 atmosphere, detecting that atmosphere through molecular features in the spectrum will require fewer transits with NIRSpec Prism* than secondary eclipses with MIRI LRS. This example demonstrates how we identify optimal observing modes for atmosphere detections and enables a comprehensive study to determine the exposure times needed to detect the presence of an atmosphere as a function of observing mode and atmosphere type.

Unless otherwise stated, throughout the rest of the paper we adopt the convention that an atmosphere is detected if $\langle \text{S}/\text{N} \rangle \geq 5$ is achieved on absorption features in the spectrum. We report our results for the detectability of atmospheres at this threshold, but encourage readers to scale our results to their own desired detection thresholds.

2.3.3. Detecting Specific Molecules

To detect individual molecules in the spectrum, we apply the methods described in the previous sections to spectra with and without the absorption features from a given molecular species. To perform these tests, we generate additional transmission and emission spectra by running our radiative transfer model for a given atmosphere with each spectrally active molecule removed one at a time. We then use the spectra that are missing contributions from individual molecules as m_2 in Equations (4) and (6) to calculate the $\langle \text{S}/\text{N} \rangle$ on the contribution from each molecule to the spectrum. In this case, rather than a “flat line” test, where we attempt to rule out a featureless spectrum and thereby detect the presence of an atmosphere, here we attempt to rule out a spectrum that does not have a particular gas—for instance H_2O —and thereby detect the presence of H_2O . This procedure enables the identification of which JWST instruments and modes are sensitive to detecting

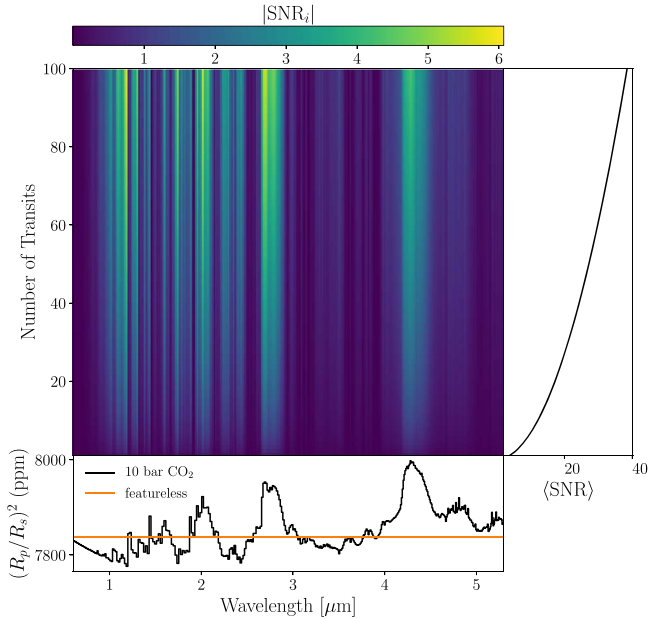


Figure 2. Signal-to-noise contours on the simulated 10 bar high CO₂ transmission spectrum, observed with *JWST*/NIRSpec Prism with six groups per integration, relative to a featureless spectrum as a function of the number of transits observed and wavelength of the instrument. The bottom panel shows the noiseless spectrum (black) and the best-fitting featureless spectrum (orange), both convolved to the instrument resolution. The right panel shows how the total expected S/N from Equation (6) increases with more transits observed.

individual molecules in an observed spectrum and how much time must be spent on any given target to reduce the noise enough to measure the spectral contributions from each molecule.

Figure 4 shows the detectability of O₂ in the atmosphere of TRAPPIST-1b with NIRSpec G140H if the planet possesses a desiccated 10 bar O₂ atmosphere. The strong O₂–O₂ collisionally induced absorption (CIA) features at 1.06 and 1.27 μm lead to a ⟨S/N⟩ = 5 detection of O₂ in seven transits. Therefore, an oxygen-dominated atmosphere for TRAPPIST-1b could be ruled out by not detecting these features in seven transits.

Unless otherwise stated, throughout the rest of the paper we adopt the convention that molecules in the atmosphere are weakly detected if ⟨S/N⟩ ≥ 3 is achieved on that molecule’s contribution to the spectrum, and we report our results for the characterization of atmospheres at this weak detection threshold. Keep in mind that we use a weaker threshold ⟨S/N⟩ to report on detecting individual molecules than for simply detecting the atmosphere, but we encourage readers to scale our molecular detection results to their own desired thresholds.

3. Results

Here we present the full results of our simulations on the detectability and characterization of the TRAPPIST-1 exoplanet atmospheres using *JWST*. First, we assess the *JWST* observations needed to detect the presence of an atmosphere for the TRAPPIST-1 planets (Section 3.1). We then address the detectability of individual molecules within the TRAPPIST-1 planet spectra that may be used to distinguish between different atmospheric states and evolutionary scenarios (Section 3.2).

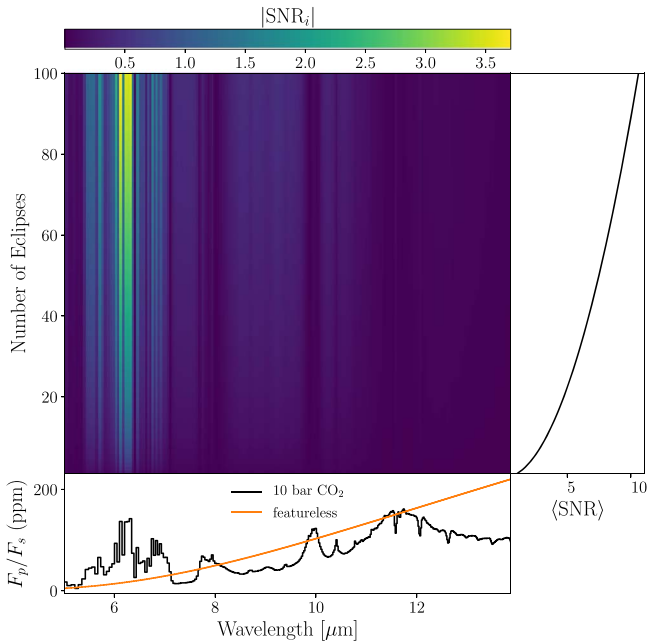


Figure 3. Signal-to-noise contours on the simulated 10 bar high CO₂ emission spectrum observed with *JWST*/MIRI/LRS relative to a featureless spectrum as a function of the number of occultations observed and wavelength of the instrument. The bottom panel shows the noiseless spectrum (black) and the best-fitting featureless spectrum (orange), both convolved to the instrument resolution. The right panel shows how the total expected S/N from Equation (6) increases with more eclipses observed.

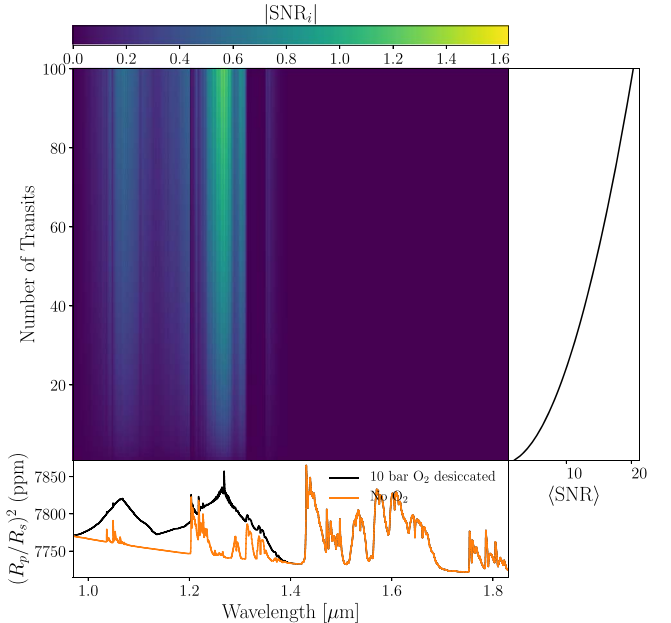


Figure 4. Signal-to-noise contours on the O₂ contribution to the transmission spectrum of TRAPPIST-1b if it possesses a 10 bar desiccated high O₂ atmosphere observed with NIRSpec G140H as a function of the number of occultations observed and wavelength of the instrument. The bottom panel shows the full model spectrum (black) and model spectrum with O₂ removed (orange), both convolved to the resolution of NIRSpec G140H. The right panel shows the total expected S/N ⟨⟨S/N⟩⟩ from Equation (6). The O₂ features at 1.06 and 1.27 μm are due to O₂–O₂ collisionally induced absorption (CIA), and could lead to ⟨⟨S/N⟩⟩ = 5 detection of O₂ in ∼7 transits.

3.1. Detecting Atmospheres

We simulate the detectability of the TRAPPIST-1 planetary atmospheres with MIRI photometry (Section 3.1.1), transmission

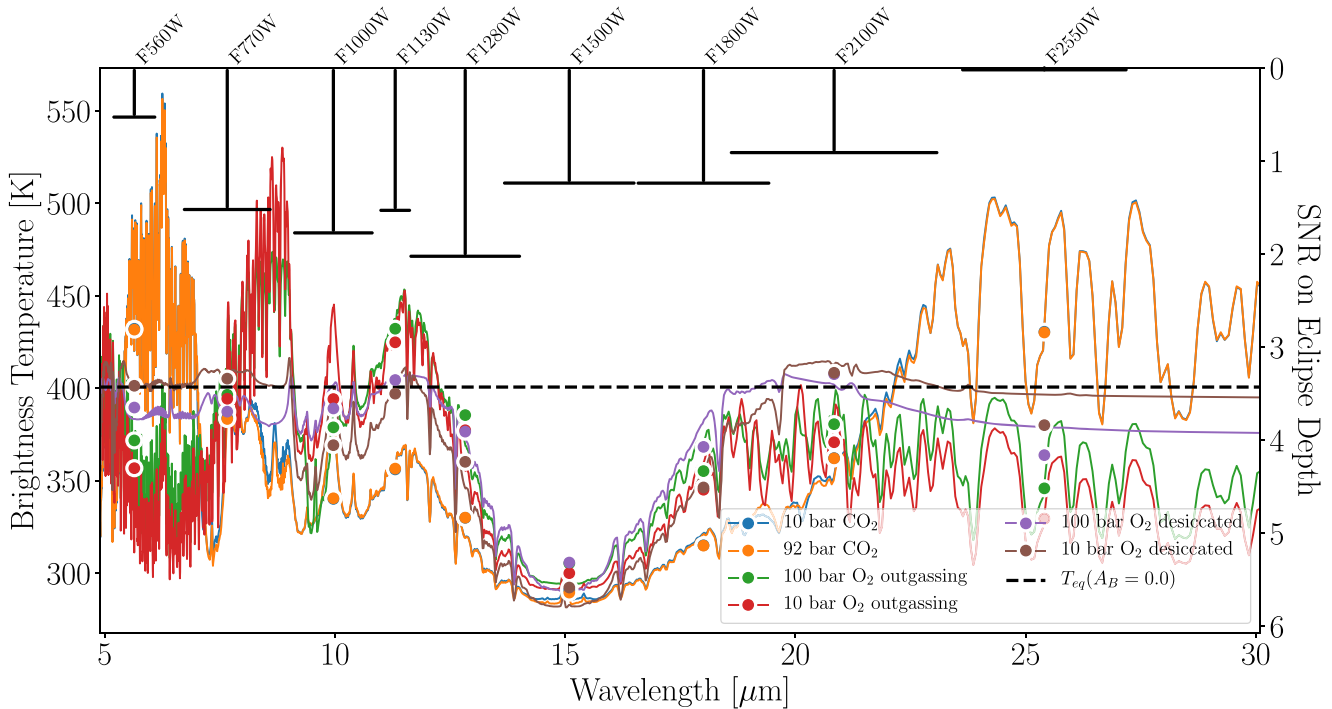


Figure 5. Brightness temperatures for different TRAPPIST-1b atmospheric models across the JWST/MIRI imaging wavelength range. The brightness temperatures integrated across each MIRI filter are shown as color points. The zero bond albedo equilibrium temperature of TRAPPIST-1b (black horizontal dashed line) is shown to compare against the model brightness temperatures, which vary as a function of wavelength due to the interplay between atmospheric temperature structure and gaseous opacities. The black lines from the top of the plot correspond to the (atmospheric model averaged) S/N on a single secondary eclipse, shown increasing from the top of the right y-axis to the bottom. These S/N indicators are shown capped with the effective width of each MIRI filter, and help to identify which filters may best offer secondary eclipse detections.

spectroscopy (Section 3.1.2), and emission spectroscopy (Section 3.1.3).

3.1.1. JWST/MIRI Photometry

MIRI photometry may be advantageous for initial assessments prior to the potentially long time commitment necessary to observe the spectrum of the Earth-sized TRAPPIST-1 planets with *JWST*. We investigate both transit and eclipse photometry with the nine MIRI photometric filters spanning wavelengths from about 5 to 27 μm (Bouchet et al. 2015). We first present results that may help to constrain the presence of an atmosphere from secondary eclipse observations in a single MIRI photometric band using brightness temperature arguments. We then present results for transit and eclipse observations in multiple filters, using the tests described in Section 2.3.2, to assess the observational requirements for ruling out a featureless spectrum.

Single-band Constraints—We calculate brightness temperatures for each of our self-consistent atmosphere models (Lincowski et al. 2018) to help plan and interpret photometric assessments of the TRAPPIST-1 planets in secondary eclipse. Figure 5 shows brightness temperature as a function of wavelength for TRAPPIST-1b for different assumed atmospheres. The wavelength-dependent fluxes were also convolved with the nine MIRI filters to calculate the brightness temperature of each atmosphere model, shown as color points in Figure 5. The horizontal dashed line shows the zero bond albedo equilibrium temperature of TRAPPIST-1b—a limit which a planet without additional internal geothermal or atmospheric greenhouse heating would not be expected to exceed. Figure 5 also provides the S/N on the depth of a single observed secondary eclipse, averaged

over the atmospheric models and displayed increasing from top to bottom on the right y-axis.

A few of the possible TRAPPIST-1b atmospheres, in particular the Venus-like and outgassing O₂ atmospheres, have brightness temperatures that exceed the zero bond albedo equilibrium temperature in a handful of the MIRI photometric bands. Like Venus, the 10 and 92 bar CO₂ atmospheres have 6 μm windows that provide a glimpse into their hotter, greenhouse-heated, lower atmospheres. The F560W MIRI filter could potentially detect this emission. The 10 and 100 bar O₂ outgassing atmospheres also have strong emission windows near 11.5 μm, between the 9.6 μm O₃ band and the 15 μm CO₂ band, which could be detected with the F1130W MIRI filter. The 10 and 92 bar CO₂ atmospheres have sufficiently strong CO₂ absorption to saturate the wings of the 15 μm band and cause a significantly lower brightness temperature at 10–12 μm compared to atmospheres not dominated by CO₂. The 10 and 92 bar CO₂ atmospheres also exceed the maximum equilibrium brightness temperature beyond about 22 μm, however the F2550W MIRI filter may lack the S/N to provide constraining information.

Despite the few cases with potentially detectable high brightness temperatures, the overwhelming majority of atmospheric models viewed through MIRI filters have brightness temperatures that are consistent with plausible planetary bond albedos (between 0 and 1), including in the 12–18 μm wavelength range where outgoing thermal radiation is strongly absorbed by the broad 15 μm CO₂ band. In the atmospheres that we considered, no single photometric band stands out above the rest as providing a definitive detection of an atmosphere via an emission window. However, secondary eclipse observations in multiple MIRI filters in and out of the

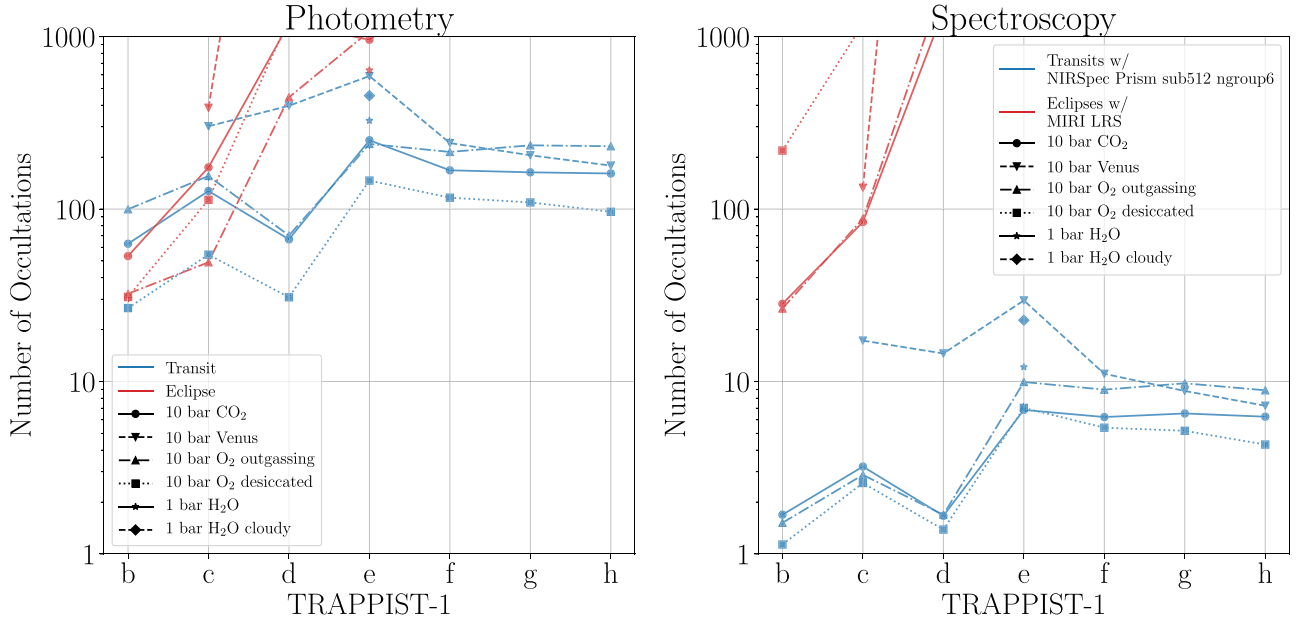


Figure 6. Number of transits (blue) or eclipses (red) needed to detect an atmosphere for all seven known TRAPPIST-1 planets with MIRI photometry (left) and *JWST* transmission spectroscopy (right). Line and marker styles designate the type of atmosphere assumed. MIRI imaging assumes that the number of occultations are split evenly between the two to three photometric filters that are optimal for detecting each atmosphere (see Section 3.1.1). Transmission spectroscopy is shown using NIRSpec Prism (see Section 3.1.2), and emission spectroscopy is shown using MIRI LRS (see Section 3.1.3). Detecting the atmospheres of the TRAPPIST-1 planets is optimal using transmission spectroscopy with NIRSpec Prism across a range of terrestrial atmospheric compositions.

strong $15\text{ }\mu\text{m}$ CO₂ feature may be used to detect the presence of an atmosphere. We discuss this point later in this section.

Although Figure 5 only shows brightness temperatures for TRAPPIST-1b, Table 3 in Appendix C lists the brightness temperature in each MIRI imaging filter for each TRAPPIST-1 planet atmosphere considered here. Table 3 also contains calculations for the Warm *Spitzer* photometric filters. We note, however, that the S/N on secondary eclipses decreases rapidly with planet equilibrium temperature, making precise eclipse photometry beyond TRAPPIST-1 c largely infeasible with *JWST*.

Multiband Constraints—We now turn to constraints that may be placed on the existence of an atmosphere using a combination of any of the nine MIRI photometric bands to observe either transits or eclipses. For each type of atmosphere, we determine the number and set of MIRI filters that can detect the atmosphere using transit and eclipse photometry in the minimum number of total occultations, assuming an equal number of occultations are observed in each filter. In all cases, two to three MIRI filters are optimal for detecting deviations from a featureless spectrum, and additional filters are costly given their marginal increase in atmospheric detectability. The F1500W filter is always optimal to include, due to the presence of CO₂ in these atmospheres. For transit photometry, the F1500W filter is best combined with F560W for CO₂-dominated atmospheres and F770W for O₂-dominated atmospheres, and typically just two filters are optimal. For eclipse photometry, the F1500W filter is best combined with F560W, F770W, and/or F1130W, and typically three filters are optimal.

The left panel of Figure 6 shows the total number of transits (blue lines) and eclipses (red lines) needed to detect different atmospheric compositions for each of the seven known TRAPPIST-1 planets using the optimal two or three MIRI photometric filters. Plotting the number of occultations (transits or eclipses) as a function of the TRAPPIST-1 planets, ordered

by semimajor axis, reveals a general trend according to the observation method: emission photometry is comparable with transmission photometry at detecting atmospheres for the innermost/hottest planets (e.g., TRAPPIST-1b and c), but becomes increasingly less efficient as the planets decrease in equilibrium temperature, whereas transmission photometry increases in observational time much more gradually with equilibrium temperature. This strong scaling with temperature occurs because the planet emission, at wavelengths contributing most to the detection of molecular features, is not in the Rayleigh–Jeans limit. The left panel of Figure 6 implies that determining whether or not the potentially habitable TRAPPIST-1 planets (e, f, and g) have atmospheres will be much more efficient with transit photometry than with eclipse photometry.

The high CO₂ atmospheres may be surprisingly difficult to distinguish with eclipse photometry because the wings of the $15\text{ }\mu\text{m}$ CO₂ band saturate and extend many microns on either side. This strong absorption effectively mutes the planet’s emitted flux, creating a nearly featureless spectrum. Consequently, MIRI eclipse photometry at $12.8\text{ }\mu\text{m}$ and $18\text{ }\mu\text{m}$ (F1280W and F1800W filters, respectively) may not be sufficiently separated from $15\text{ }\mu\text{m}$ (F1500W) to avoid substantial contamination from the wings of strong CO₂ absorption (see the orange curve in Figure 5), making these filters ineffective for continuum measurement. Instead, the F1130W filter may be better at probing deeper into the atmosphere.

3.1.2. JWST Transmission Spectroscopy

We now present results on the detectability of the TRAPPIST-1 planet atmospheres using transmission spectroscopy with *JWST*. We begin with a few specific examples of detectable TRAPPIST-1 atmospheres to demonstrate the size of molecular absorption features relative to the expected *JWST*

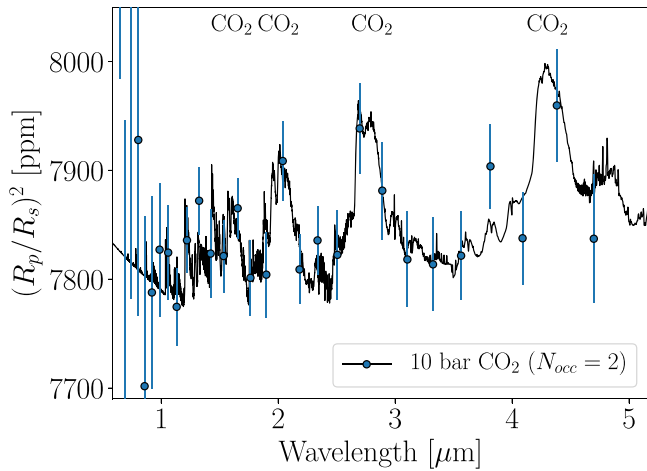


Figure 7. Model transmission spectrum of TRAPPIST-1b with a 10 bar CO₂ atmosphere. Synthetic data are simulated for two transits observed with NIRSpec Prism* and binned to a resolution of $R = 8$.

noise, and then present our full ensemble of results for each TRAPPIST-1 planet, atmosphere, and *JWST* instrument.

Specific Examples of Atmospheric Detection—Figure 7 shows an example detection of absorption features in the transmission spectrum of TRAPPIST-1b assuming it possesses a clear 10 bar CO₂ atmosphere. The transmission spectrum is shown with synthetic data simulated for two transits observed with NIRSpec Prism*, which we find to be sufficient to rule out a featureless spectrum with $\langle S/N \rangle = 5$ (our fiducial detection limit). The synthetic data are shown binned to a resolution of $R = 8$; however, the featureless spectrum was ruled out at the native resolution of NIRSpec Prism ($R \approx 100$). CO₂ absorption features at 1.6, 2.0, 2.8, and 4.3 μm drive the detectability of this atmosphere and are apparent in the synthetic data.

Figure 8 demonstrates possible transmission spectra of TRAPPIST-1c for two different aerosol conditions. Both cases are CO₂-dominated spectral models from Lincowski et al. (2018) with simulated noise for observations with NIRSpec Prism*. The number of transits observed for each model is calculated such that the atmosphere is strongly detected with $\langle S/N \rangle = 10$. The blue model shows a clear-sky spectrum with large CO₂ absorption features and data uncertainties calculated for 16 observed transits. The red model includes H₂SO₄ clouds at altitudes consistent with H₂SO₄ condensation, with data uncertainties calculated for 72 observed transits.

The aerosol-free atmosphere has strong CO₂ features that can be detected in considerably fewer transits than the case with Venus-like H₂SO₄ aerosols. The self-consistent clouds are located high enough in the atmosphere that over 70 transits are required to detect the CO₂ absorption features with the same confidence as the clear-sky case. If TRAPPIST-1c possesses Venus-like aerosols, then about 5× more transits than our estimates for the clear-sky case must be observed to achieve comparable constraints on the presence and composition of TRAPPIST-1c's atmosphere.

We find a factor of ∼4 variation in the number of transits needed to detect the atmosphere of TRAPPIST-1e depending on the type of terrestrial atmosphere it possesses. Figure 9 explores the detectability of molecular features in the transmission spectrum of TRAPPIST-1e. Like Figure 8, Figure 9 shows possible TRAPPIST-1e model spectra with simulated NIRSpec Prism* observations assuming the number

of transits needed to strongly detect features in each atmosphere with $\langle S/N \rangle \approx 10$. Spectra for water-covered environments with and without a water cloud are shown in teal and blue, respectively, and CO₂-dominated atmospheres, with and without H₂SO₄ aerosols, are shown in orange and red, respectively. To detect features in each spectrum with $\langle S/N \rangle \approx 10$ ($\langle S/N \rangle \approx 5$), and thereby obtain approximately equal constraints on the presence of TRAPPIST-1's atmosphere, will require ∼30 (∼7) transits for a clear-sky CO₂ atmosphere, ∼50 (∼13) transits for a clear-sky aqua planet atmosphere, ∼90 (∼22) transits for a cloudy aqua planet atmosphere, and ∼120 (∼30) transits for a CO₂-dominated atmosphere with H₂SO₄ clouds.

Optimal JWST Observing Modes for Atmospheric Detection

—Thus far we have only discussed specific cases for the detectability of the TRAPPIST-1 planet atmospheres with *JWST* transmission spectroscopy; we now report results from our comprehensive study to determine the exposure times needed to detect the presence of atmospheres as a function of *JWST* observing mode and atmosphere type, for each TRAPPIST-1 planet. The number of transits necessary to detect spectral features in the transmission spectrum with $\langle S/N \rangle = 5$ for TRAPPIST-1b, c, d, e, f, g, and h are shown in Appendix B in Figures 13–19, respectively, as a function of both atmospheric compositions and *JWST* instrument/mode. Color is used in these figures to guide the eye to small (more blue) and large (more white) values for the number of transits.

These results suggest that under most circumstances, the *JWST*/NIRSpec Prism is the optimal instrument for detecting the presence of an atmosphere using transmission spectroscopy of the TRAPPIST-1 planets. If a partial saturation strategy is used with NIRSpec Prism (Batalha et al. 2018), then it will be more capable of detecting atmospheric features than any other *JWST* instrument or mode. However, if it turns out that the systematics introduced via partial saturation are not beneficial, the SUB512S subarray will offer improved performance over the SUB512 subarray, due to its shorter readout time. We note, though, that SUB512 should be considered the subarray of choice because SUB512s has limited access to important background pixels, and it may be difficult to keep the curved trace inside only 16 pixels in the cross-dispersion direction. The NIRSpec G395M/H disperser offers comparable results with the standard (no partial saturation) NIRSpec Prism.

Most of the atmospheres that we consider may require fewer than 12 transits to be detected for all of the TRAPPIST-1 planets using the optimized NIRSpec Prism mode. Figure 10 displays the number of transits to detect the TRAPPIST-1 planet atmospheres using only the NIRSpec Prism* instrument for each TRAPPIST-1 planet and for each atmosphere considered in this work.

Our results show that the outer TRAPPIST-1 planets require only two to seven more transits than TRAPPIST-1b to detect clear-sky atmospheres. The right panel of Figure 6 summarizes the best-case scenario results for detecting the atmospheres of the TRAPPIST-1 planets with *JWST* transit spectroscopy (blue lines). The number of transits required to detect the atmosphere at $\langle S/N \rangle = 5$ for each of the atmospheric models is shown for observations with NIRSpec Prism*. Like our transit photometry results, the number of transits only weakly increases with semimajor axis. However, significantly fewer transits are required for transmission spectroscopy atmosphere detections with NIRSpec Prism* than with MIRI filter photometry. The

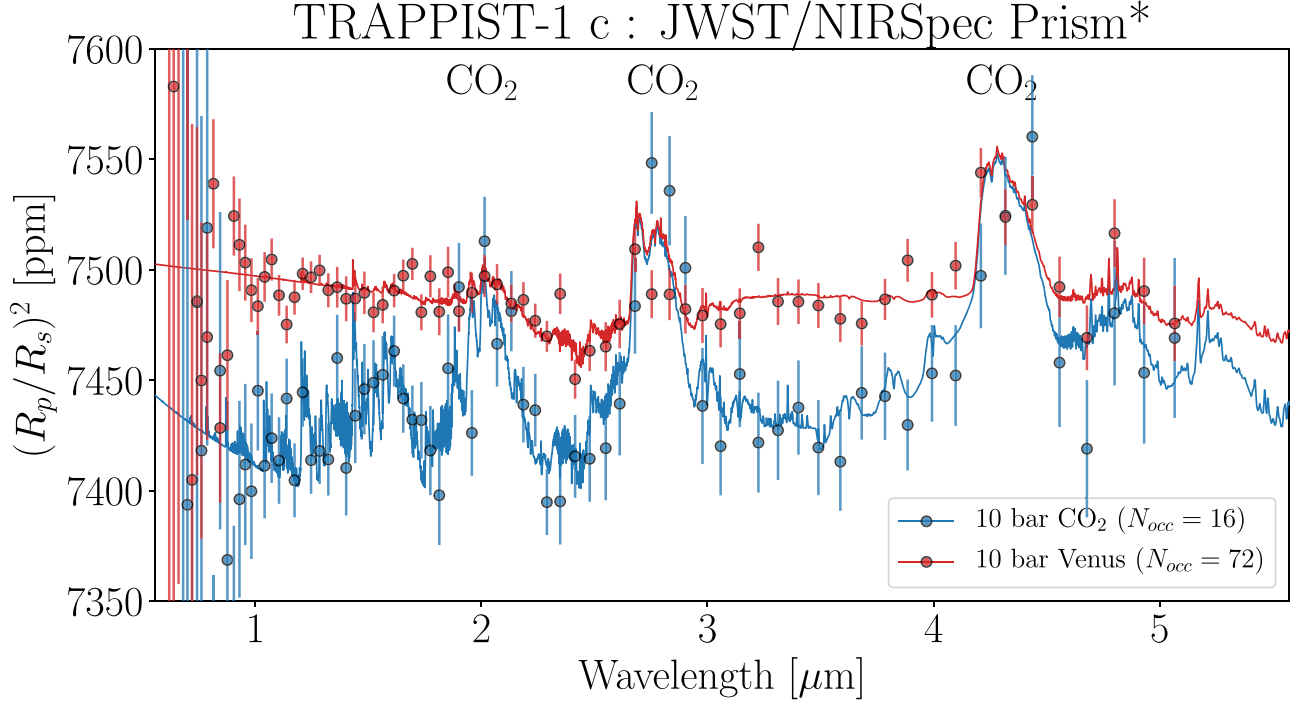


Figure 8. Simulated JWST/NIRSpec Prism transmission spectra of TRAPPIST-1c for different CO₂-dominated atmospheric states. The blue model shows a clear-sky spectrum with large CO₂ absorption features, and the red model includes a self-consistent H₂SO₄ cloud. The number of coadded transits simulated for each NIRSpec observation is set so that the atmosphere is strongly detected ($\langle S/N \rangle = 10$). That is, to obtain approximately equal constraints on the presence and composition of TRAPPIST-1c's atmosphere will require 16 transits for the clear-sky CO₂ case and 72 transits for the cloudy case.

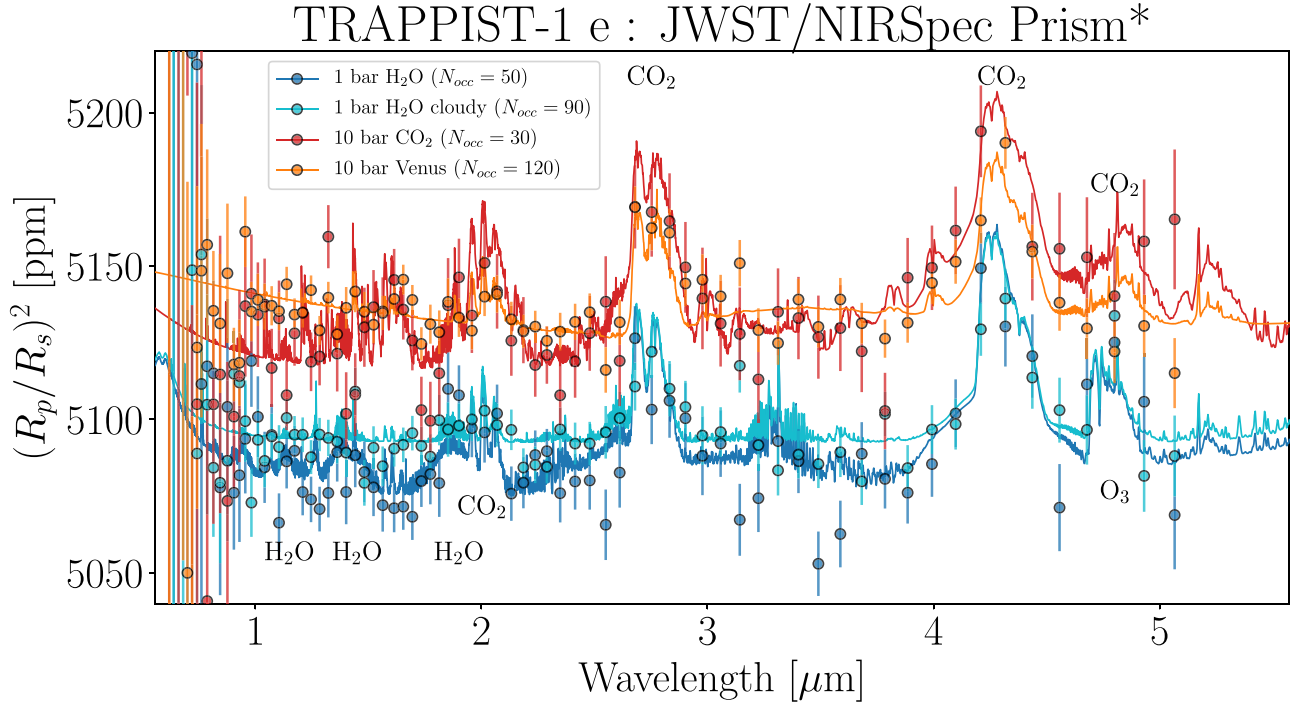


Figure 9. Simulated JWST/NIRSpec Prism* transmission spectra of TRAPPIST-1e for different possible atmospheric compositions. The teal and blue models show spectra for water-dominated atmospheres, with and without a water cloud, respectively. The orange and red spectra are for CO₂-dominated atmospheres, with and without H₂SO₄ aerosols, respectively. The number of coadded transits simulated for each NIRSpec observation is set so that the atmosphere is strongly detected ($\langle S/N \rangle = 10$). That is, to obtain approximately equal constraints on the presence of TRAPPIST-1e's atmosphere will require ~ 30 transits for a clear-sky CO₂ atmosphere, ~ 50 transits for a clear-sky H₂O atmosphere, ~ 90 transits for a cloudy H₂O atmosphere, and ~ 120 transits for a CO₂-dominated Venus-like atmosphere.

emission spectroscopy results in Figure 6 (red lines) are discussed in Section 3.1.3.

The atmospheric composition of the planets has a relatively minimal effect on the number of transits needed to rule out a

featureless spectrum, with Venus-like clouds being a significant exception. All atmospheric cases considered for TRAPPIST-1c could be detected in three to four transits with NIRSpec Prism*, except for the 10 and 92 bar Venus atmospheres (with H₂SO₄

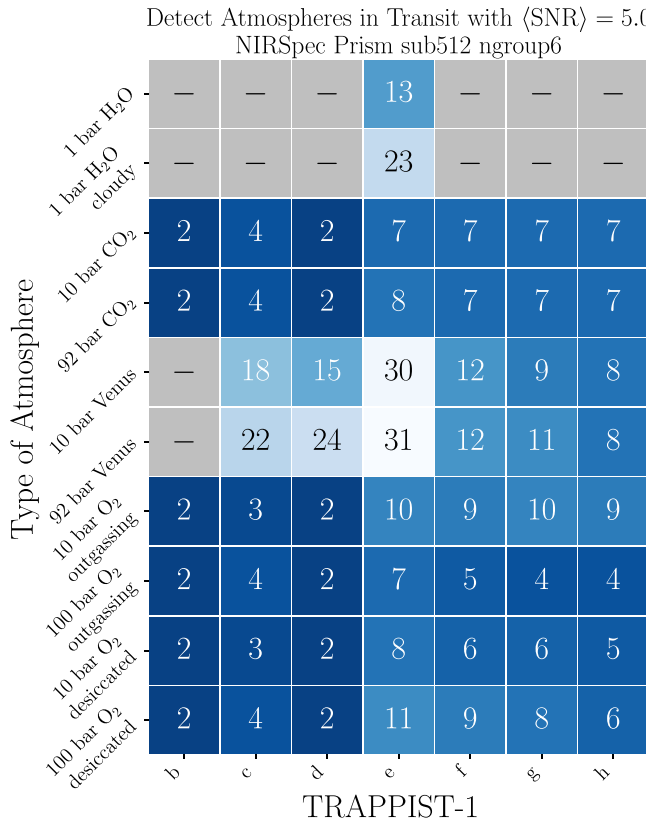


Figure 10. Number of transits for each TRAPPIST-1 planet necessary to rule out a featureless spectrum with $\langle S/N \rangle = 5$ for different self-consistent atmospheric compositions using *JWST* NIRSpec Prism with the partial saturation mode of Batalha et al. (2018).

aerosols), which would require $4.5\times$ and $5.5\times$ the number of transits to detect, respectively, compared to the 10 and 92 bar clear-sky CO₂ counterparts. In general, more transits tend to be required to detect the atmospheres of the cooler worlds, except for TRAPPIST-1d, which is more comparable to TRAPPIST-1b in the detectability of its atmosphere. While the atmosphere of TRAPPIST-1d may be relatively easy to detect if it is without clouds, with clouds, the 10 and 92 bar CO₂ atmospheres require $7.5\times$ and $12\times$ the number of transits to detect, respectively, the largest increase due to clouds seen in the sample. Beyond TRAPPIST-1e, the effect of Venus-like clouds has a diminished impact on the atmospheric detectability, with fewer than $2\times$ the number of transits required to detect the atmospheres for TRAPPIST-1f, g, and h if they have clouds.

Note that the numerical values in Figures 10 and 13–19 can easily be scaled to higher or lower $\langle S/N \rangle$ thresholds that more or less confidently rule out a featureless spectrum. Because the S/N on an observation (and $\langle S/N \rangle$) scales with the square root of the exposure time, and the number of occultations is a proxy for exposure time, we can obtain a new value for the number of occultations,

$$N'_{\text{occ}} = N_{\text{occ}} \left(\frac{\langle S/N \rangle'}{\langle S/N \rangle} \right)^2, \quad (10)$$

where N_{occ} is the number of occultations necessary to distinguish features in the spectrum with $\langle S/N \rangle$ (5 in Figures 10, 13–19) and $\langle S/N \rangle'$ is the new S/N threshold.

The increased transit duration with semimajor axis makes our results for the outer TRAPPIST-1 planets appear more optimistic

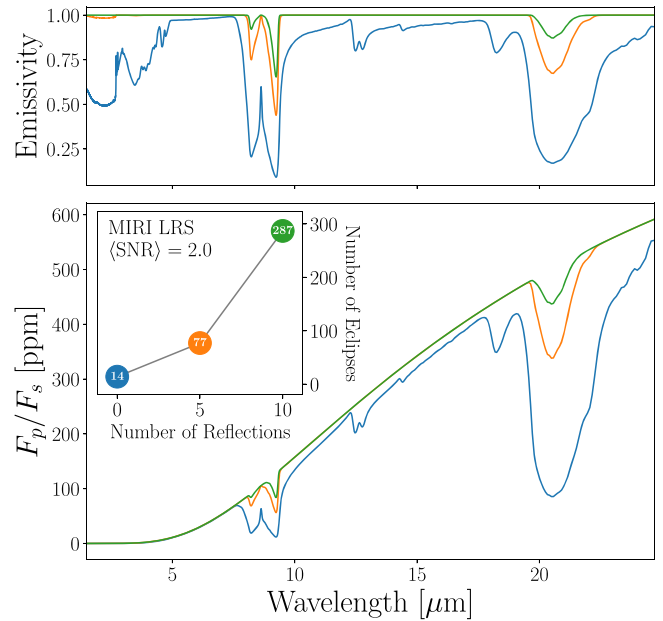


Figure 11. Estimated detectability of pure quartz surface emissivity features in the secondary eclipse spectrum of TRAPPIST-1b with *JWST*'s MIRI LRS instrument. The top panel shows the MIR effective emissivity of a quartz surface for three different assumed values for the number of surface reflections (see Equation (9)): 0 (blue), 5 (orange), and 10 (green). The bottom panel shows theoretical secondary eclipse spectra for TRAPPIST-1b assuming the effective emissivities from the top panel. The inset axis shows the number of secondary eclipses that would be required to be observed with MIRI LRS to detect features in the emission spectrum with $\langle S/N \rangle = 2.0$, for each of the three assumed effective emissivities. Only an extremely polished pure quartz surface could possibly be detected with *JWST*.

relative to our results for the inner planets. Note that for *JWST* planning, our reported number of transits/eclipses leads to different telescope times for each TRAPPIST-1 planet because each has a different transit duration. For each observed transit (eclipse), we assumed one transit duration worth of out-of-transit (out-of-eclipse) observing time. Considering the following median transit durations for the TRAPPIST-1 planets from Grimm et al. (2018): 36.40 minutes for b, 42.37 minutes for c, 49.13 minutes for d, 57.21 minutes for e, 62.60 minutes for f, 68.40 minutes for g, and 76.7 minutes for h, one can calculate the expected on-target time per transit/eclipse (before overheads) by multiplying the transit duration by two plus any overheads.

JWST is not always able to point at TRAPPIST-1 due to the star's proximity to the ecliptic plane. As a result, the star will only be observable to *JWST* for ~ 100 days per year.⁶ Over the course of *JWST*'s nominal 5 yr mission, the maximum number of observable transits/eclipses is approximately: 331 for b, 206 for c, 123 for d, 81 for e, 54 for f, 40 for g, and 26 for h. Of course, an extended mission lifetime would allow considerably more observations of the TRAPPIST-1 system.

3.1.3. JWST Emission Spectroscopy

Unlike transmission spectroscopy, which can make use of many *JWST* instruments that span a broad wavelength range (e.g., NIRCam, NIRSpec, NIRISS, and MIRI LRS), secondary eclipse spectroscopy of the TRAPPIST-1 planets will only be viable at the longer wavelengths accessible to *JWST*. This is primarily

⁶ <https://jwst-docs.stsci.edu/display/JTI/JWST+Target+Viewing+Constraints>

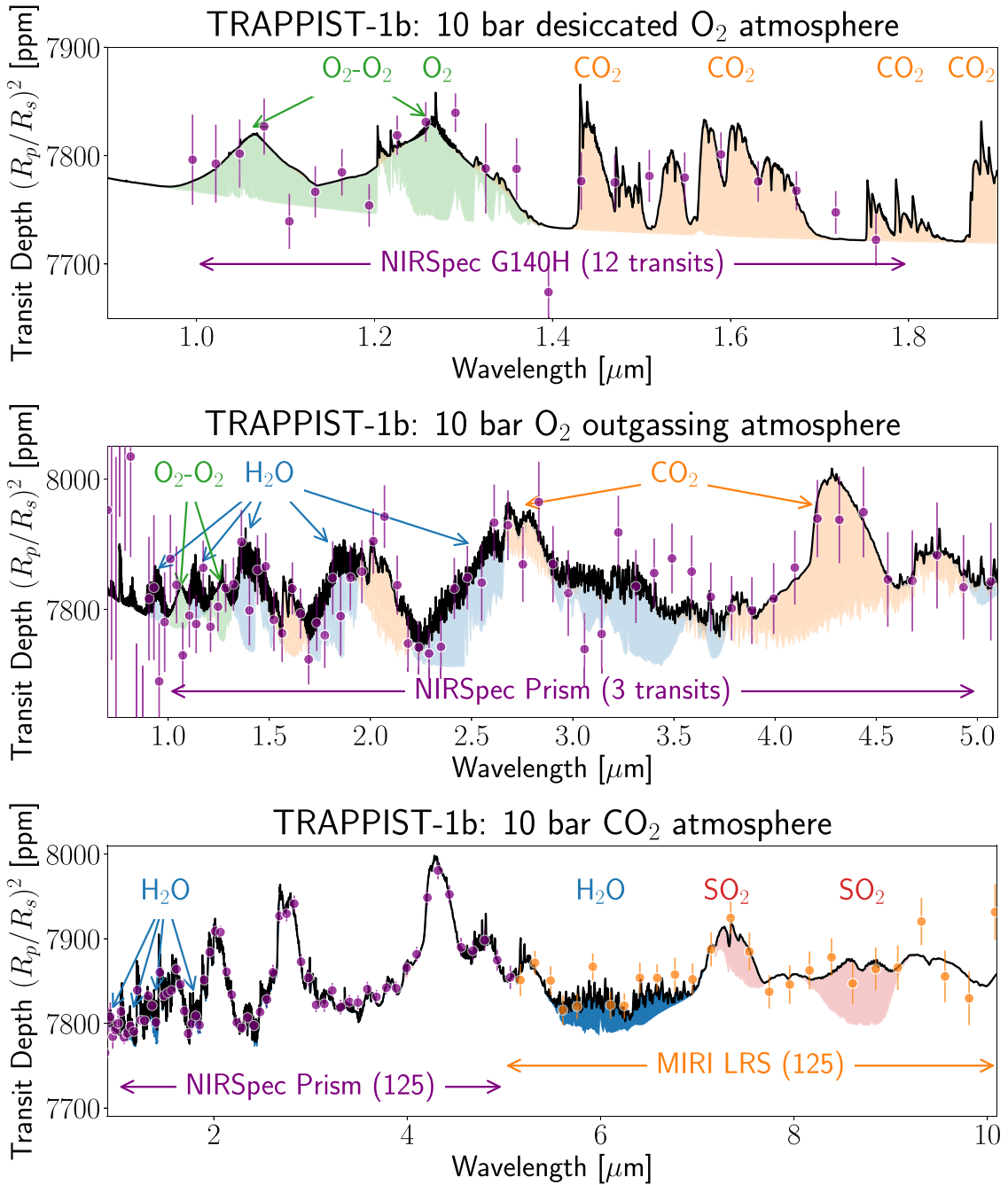


Figure 12. Theoretical transmission spectra of TRAPPIST-1b assuming three different atmospheric compositions with modeled noise for *JWST* observations. Top: transmission spectrum of a 10 bar desiccated O₂ atmosphere shown with error bars calculated for 12 transits with NIRSpec G140H—sufficient for $\langle S/N \rangle \sim 5$ on the O₂ features. Middle: transmission spectrum of a 10 bar outgassing O₂ atmosphere shown with error bars calculated for three transits with NIRSpec Prism*—sufficient for $\langle S/N \rangle \sim 5$ on the H₂O features. Bottom: transmission spectrum of a 10 bar CO₂ atmosphere shown with error bars calculated for 125 transits with NIRSpec Prism*—sufficient for $\langle S/N \rangle \sim 5$ on the NIR H₂O features—and 125 transits with MIRI LRS—sufficient for $\langle S/N \rangle \sim 5$ on both the 6 μm H₂O feature and the 7.3 and 8.7 μm SO₂ features.

driven by the increase in eclipse depths with wavelength as the planet-star contrast ratio becomes more favorable.

We find that only MIRI LRS observations of TRAPPIST-1b and c may potentially rule out a featureless emission spectrum with $\langle S/N \rangle = 5$ in fewer than 100 observed secondary eclipses. Using an analogous approach to that shown in Figures 13–19, MIRI LRS observations of TRAPPIST-1b may rule out a featureless emission spectrum in 27–47 secondary eclipses if the planet possesses a (10 or 92 bar) clear-sky CO₂ atmosphere or an (10 or 100 bar) outgassing O₂ atmosphere,

with the 10 bar outgassing O₂ atmosphere the most readily detectable. Over 100 secondary eclipses are required if the planet possesses a desiccated O₂ atmosphere (10 or 100 bars), as these emission spectra appear remarkably featureless between 5 and 9 μm . For TRAPPIST-1c we find that MIRI LRS observations could rule out a featureless emission spectrum in 85–100 secondary eclipses if the planet possesses a (10 or 92) bar clear CO₂ atmosphere or a 10 bar O₂ atmosphere with outgassing. Over 100 secondary eclipses are required for all other atmospheric compositions considered for

TRAPPIST-1c, including the CO₂ atmospheres with H₂SO₄ clouds, which have emission spectra similar to the clear CO₂ atmospheres, but with reduced temperature contrasts in the absorbing and emitting spectral regions that effectively mute the features and drive the spectrum toward a featureless blackbody. All of the exterior TRAPPIST-1 planets have emission spectra that will appear indistinguishable from cool blackbodies, due to insufficient S/N.

The right panel of Figure 6 summarizes the best-case scenario results for detecting the atmospheres of the TRAPPIST-1 planets with *JWST* emission spectroscopy (red lines) to compare against our filter photometry and transmission spectroscopy results. The number of eclipses required to detect the atmosphere at $\langle S/N \rangle = 5$ for each of the atmospheric models is shown for observations with MIRI LRS. Compared with transmission spectroscopy, emission spectroscopy is an inefficient method for detecting the TRAPPIST-1 planetary atmospheres, particularly for the cooler planets.

If TRAPPIST-1b does not possess an atmosphere, emissivity features from minerals on the surface of the planet are not likely to be detectable in secondary eclipse thermal emission spectra. Figure 11 shows the estimated thermal emission spectrum of TRAPPIST-1b if it is airless and possesses a pure quartz surface. Three different effective emissivities are shown in the top panel, corresponding to 0 (blue), 5 (orange), and 10 (green) surface reflections (see Equation (9)). The bottom panel shows the MIR secondary eclipse spectrum for each surface emissivity, assuming the surface is at the (highly optimistic) zero bond albedo equilibrium temperature for TRAPPIST-1b (392 K). The inset axis shows the number of secondary eclipses that MIRI LRS would have to observe to detect features in each emission spectrum at a weak $\langle S/N \rangle = 2.0$. Increasing the number of surface reflections results in surface emissivity features that are not detectable.

3.2. Distinguishing Specific Molecules

We now present the sensitivity of each *JWST* instrument to each gas in the Lincowski et al. (2018) TRAPPIST-1 model transmission spectra. Table 2 lists the molecules for which *JWST* could weakly detect ($\langle S/N \rangle = 3.0$) that molecule's contribution to the spectrum in 100 or fewer transits. For each molecule, the number of transits is listed in parentheses next to each molecular formula along with a footnote identifying which *JWST* instrument is used for that observation. While in some cases multiple instruments may be sensitive to the same molecule, we list only the instrument that can detect each gas in the minimum number of transits.

The presence of CO₂ dominates the detectability of all the atmospheres simulated in Lincowski et al. (2018) with *JWST*. Even a relatively small amount of CO₂ (e.g., ~ 290 ppm for the 1 bar H₂O TRAPPIST-1e) can saturate the strong 2.7, 4.3, and 15 μm CO₂ absorption features and lead to the detection of both the atmosphere and CO₂. As a result, the number of transits necessary to detect spectral features in a transmission spectrum, given in Section 3.1.2, is close to the number of transits necessary to detect CO₂. In some cases, the number of transits to detect CO₂ is fewer than that needed to simply detect the atmosphere. This is because the spectral model without CO₂ deviates more significantly from the true spectrum than the best-fitting featureless spectrum. In these cases, it is important to defer to the number of transits required to rule out a featureless spectrum, because it provides a more realistic fit to the spectrum.

Table 2
Detectable Molecules with Transmission Spectroscopy for Different Plausible TRAPPIST-1 Planet Atmospheres

Planet	Model	Molecules (Number of transits to $\langle S/N \rangle = 3.0$)
T-1b	10 bar CO ₂	CO ₂ (1 ^c), CO(47 ^c), H ₂ O(44 ^d), SO ₂ (40 ^d)
	92 bar CO ₂	CO ₂ (1 ^c), CO(47 ^c), H ₂ O(41 ^d), SO ₂ (38 ^d)
	100 bar O ₂ outgassing	CO ₂ (1 ^c), H ₂ O(2 ^e), O ₃ (11 ^c), O ₂ (3 ^a)
	10 bar O ₂ outgassing	CO ₂ (1 ^c), H ₂ O(1 ^b), O ₂ (4 ^a)
	100 bar O ₂ desiccated	CO ₂ (1 ^c), O ₂ (3 ^a)
	10 bar O ₂ desiccated	CO(13 ^b), CO ₂ (1 ^c), O ₃ (81 ^d), O ₂ (3 ^a)
	10 bar CO ₂	CO ₂ (1 ^c), H ₂ O(45 ^d), SO ₂ (51 ^d)
	92 bar CO ₂	CO ₂ (1 ^c), H ₂ O(43 ^d), SO ₂ (52 ^d)
	100 bar O ₂ outgassing	CO ₂ (3 ^c), H ₂ O(4 ^e), O ₃ (5 ^c), O ₂ (7 ^a)
	10 bar O ₂ outgassing	CO ₂ (2 ^c), H ₂ O(2 ^e), O ₃ (86 ^d), O ₂ (5 ^a)
T-1c	100 bar O ₂ desiccated	CO ₂ (2 ^c), O ₃ (71 ^d), O ₂ (7 ^a)
	10 bar O ₂ desiccated	CO(61 ^e), CO ₂ (1 ^c), O ₃ (64 ^d), O ₂ (6 ^a)
	10 bar Venus	CO ₂ (3 ^c)
	92 bar Venus	CO ₂ (6 ^c)
	10 bar CO ₂	CO ₂ (1 ^c), CO(48 ^e), H ₂ O(18 ^d), SO ₂ (27 ^d)
	92 bar CO ₂	CO ₂ (1 ^c), CO(47 ^e), H ₂ O(17 ^d), SO ₂ (27 ^d)
	100 bar O ₂ outgassing	CO ₂ (2 ^c), H ₂ O(2 ^e), O ₃ (2 ^c), O ₂ (3 ^a)
	10 bar O ₂ outgassing	CO ₂ (1 ^c), H ₂ O(2 ^e), O ₃ (32 ^d), O ₂ (3 ^a)
	100 bar O ₂ desiccated	CO ₂ (1 ^c), O ₃ (26 ^d), O ₂ (3 ^a)
	10 bar O ₂ desiccated	CO(49 ^e), CO ₂ (1 ^c), O ₃ (30 ^d), O ₂ (3 ^a)
T-1d	10 bar Venus	CO ₂ (6 ^c)
	92 bar Venus	CO ₂ (7 ^c)
	10 bar CO ₂	CO ₂ (2 ^c), SO ₂ (86 ^d)
	92 bar CO ₂	CO ₂ (2 ^c), SO ₂ (88 ^d)
	100 bar O ₂ outgassing	CO ₂ (9 ^c), H ₂ O(64 ^e), O ₃ (4 ^e), O ₂ (22 ^a)
	10 bar O ₂ outgassing	CO ₂ (4 ^c), H ₂ O(78 ^e), O ₃ (72 ^c), O ₂ (24 ^a)
	100 bar O ₂ desiccated	CO ₂ (4 ^c), O ₃ (61 ^d), O ₂ (18 ^a)
	10 bar O ₂ desiccated	CO ₂ (3 ^c), O ₃ (40 ^e), O ₂ (19 ^a)
	10 bar Venus	CO ₂ (9 ^c)
	92 bar Venus	CO ₂ (9 ^c)
T-1e	1 bar H ₂ O	CO ₂ (9 ^c), H ₂ O(15 ^e), N ₂ (68 ^c)
	1 bar H ₂ O cloudy	CO ₂ (13 ^c)
	10 bar CO ₂	CO ₂ (2 ^c), SO ₂ (76 ^d)
	92 bar CO ₂	CO ₂ (2 ^c), SO ₂ (79 ^d)
	100 bar O ₂ outgassing	CO ₂ (7 ^c), O ₃ (2 ^c), O ₂ (23 ^a)
	10 bar O ₂ outgassing	CO ₂ (4 ^c), O ₃ (39 ^e), O ₂ (30 ^d)
	100 bar O ₂ desiccated	CO ₂ (4 ^c), O ₃ (10 ^e), O ₂ (20 ^a)
	10 bar O ₂ desiccated	CO ₂ (3 ^c), O ₃ (7 ^c), O ₂ (20 ^a)
	10 bar Venus	CO ₂ (3 ^c)
	92 bar Venus	CO ₂ (3 ^c)
T-1f	10 bar CO ₂	CO ₂ (2 ^c), SO ₂ (82 ^d)
	92 bar CO ₂	CO ₂ (2 ^c), SO ₂ (89 ^d)
	100 bar O ₂ outgassing	CO ₂ (9 ^c), O ₃ (2 ^c), O ₂ (36 ^a)
	10 bar O ₂ outgassing	CO ₂ (4 ^c), O ₃ (29 ^e), O ₂ (43 ^a)
	100 bar O ₂ desiccated	CO ₂ (5 ^c), O ₃ (6 ^c), O ₂ (28 ^a)
	10 bar O ₂ desiccated	CO ₂ (3 ^c), O ₃ (5 ^e), O ₂ (28 ^a)
	10 bar Venus	CO ₂ (3 ^c)
	92 bar Venus	CO ₂ (3 ^c)
	10 bar CO ₂	CO ₂ (2 ^c), SO ₂ (85 ^d)
	92 bar CO ₂	CO ₂ (2 ^c), SO ₂ (86 ^d)
T-1g	100 bar O ₂ outgassing	CO ₂ (9 ^c), O ₃ (1 ^c), O ₂ (32 ^a)
	10 bar O ₂ outgassing	CO ₂ (4 ^c), O ₃ (39 ^e), O ₂ (20 ^a)
	100 bar O ₂ desiccated	CO ₂ (4 ^c), O ₃ (10 ^e), O ₂ (20 ^a)
	10 bar O ₂ desiccated	CO ₂ (3 ^c), O ₃ (7 ^c), O ₂ (20 ^a)
	10 bar Venus	CO ₂ (3 ^c)
	92 bar Venus	CO ₂ (3 ^c)
	10 bar CO ₂	CO ₂ (2 ^c), SO ₂ (82 ^d)
	92 bar CO ₂	CO ₂ (2 ^c), SO ₂ (89 ^d)
	100 bar O ₂ outgassing	CO ₂ (9 ^c), O ₃ (2 ^c), O ₂ (36 ^a)
	10 bar O ₂ outgassing	CO ₂ (4 ^c), O ₃ (29 ^e), O ₂ (43 ^a)
T-1h	100 bar O ₂ desiccated	CO ₂ (5 ^c), O ₃ (6 ^c), O ₂ (28 ^a)
	10 bar O ₂ desiccated	CO ₂ (3 ^c), O ₃ (5 ^e), O ₂ (28 ^a)
	10 bar Venus	CO ₂ (2 ^c)
	92 bar Venus	CO ₂ (2 ^c)
	10 bar CO ₂	CO ₂ (2 ^c), SO ₂ (85 ^d)
	92 bar CO ₂	CO ₂ (2 ^c), SO ₂ (86 ^d)
	100 bar O ₂ outgassing	CO ₂ (9 ^c), O ₃ (1 ^c), O ₂ (32 ^a)
	10 bar O ₂ outgassing	CO ₂ (4 ^c), SO ₂ (54 ^d), O ₃ (23 ^c), O ₂ (31 ^a)
	100 bar O ₂ desiccated	CO ₂ (4 ^c), O ₃ (3 ^c), O ₂ (22 ^a)
	10 bar O ₂ desiccated	CO ₂ (3 ^c), O ₃ (4 ^e), O ₂ (22 ^a)

Notes.

^a NIRSpec G140H.

^b NIRSpec G235H.

^c NIRSpec G395H.

^d MIRI LRS.

^e NIRSpec Prism sub512 ngroup6.

The inner TRAPPIST-1 planets may have several detectable molecules that can be used to distinguish between different evolutionary scenarios. H₂O and SO₂ may be marginally detectable with MIRI LRS transmission spectra of the inner TRAPPIST-1 planets—b, c, and d—if they possess clear-sky CO₂ atmospheres. However, if these planets possess H₂SO₄ clouds, then H₂O and SO₂ may be undetectable. Alternatively, if TRAPPIST-1b, c, and d have oxygen-dominated atmospheres then O₂ should be distinguishable via O₂–O₂ (O₄) CIA features at 1.06 and 1.27 μm , which are slightly more detectable with NIRSpec G140M/H than NIRSpec Prism*. An oxygen-dominated planet with outgassing may be distinguished from a completely desiccated world by detecting H₂O, which is only readily detectable in our models of O₂ planets with outgassing.

TRAPPIST-1e offers an opportunity to characterize a planet in the habitable zone with *JWST*. Like the inner TRAPPIST-1 planets, O₂ may be detectable in the spectrum of an oxygen-dominated atmosphere via the O₂–O₂ CIA features. However, modern Earth levels of O₂ and O₃, and Earth geologic levels of CH₄ in a 1 bar N₂-dominated atmosphere are not likely to be detectable. If TRAPPIST-1e possesses such a habitable environment without clouds, tropospheric H₂O may be detectable using NIRSpec Prism*. However, with full cloud coverage the detectability of H₂O strongly diminishes and becomes unobservable. The broad 4.3 μm N₂–N₂ CIA feature may be marginally detectable in a 1 bar habitable N₂-dominated atmosphere with NIRSpec G395M/H. The 9.6 μm O₃ feature would require just over 100 transits with MIRI LRS to be detected at $\langle \text{S/N} \rangle = 3.0$ in the clear-sky 1 bar N₂-dominated atmosphere; approximately twice the number of transits would be required if the planet possesses 100% water cloud coverage.

For the outer planets—TRAPPIST-1f, g, and h—modest atmospheric characterization with transmission spectroscopy may be possible. In particular, oxygen-dominated atmospheres may be distinguished not only by their prominent O₂–O₂ CIA features, but also by their O₃ features, which become more detectable than the O₂–O₂ features for the coolest TRAPPIST-1 planets with NIRSpec Prism*.

The observational difficulty with which individual molecules may be detected in a transmission spectrum—bulk atmospheric constituents or trace gases—varies substantially as a function of atmospheric composition. Consequently, the gases that are both relatively easy to detect and unique to a specific atmosphere make optimal testable hypotheses for that atmospheric composition. Figure 12 demonstrates a potential approach for distinguishing among three different atmospheric states for TRAPPIST-1b using *JWST* transmission spectroscopy. The models are shown with calculated error bars that correspond to the amount of *JWST* observing time that would be required to detect specific molecules in the given spectrum.

In the top panel of Figure 12, the spectrum of a 10 bar desiccated oxygen atmosphere displays prominent O₄ features that may be detected with $\langle \text{S/N} \rangle \sim 5$ in 12 transits with NIRSpec G140H. This is a strong discriminant between an O₂-dominated atmosphere and a CO₂-dominated atmosphere, both of which have strong and detectable CO₂ features.

The spectrum of a 10 bar oxygen atmosphere with outgassing is shown in the middle panel of Figure 12. This spectrum has detectable O₄ features similarly to the desiccated atmosphere, but also substantial H₂O features (due to Earth levels of geological fluxes) that may be detected with

$\langle \text{S/N} \rangle \sim 5$ in just three transits with NIRSpec Prism*. Such strong water absorption in an oxygen-dominated atmosphere would indicate incomplete desiccation.

The spectrum of a 10 bar CO₂ atmosphere is shown in the bottom panel of Figure 12. This spectrum contrasts with the outgassing oxygen atmosphere in the detectability of H₂O. Water in a Venus-like atmosphere is scarce, particularly in the upper atmosphere, which would require ~ 125 transits with either NIRSpec Prism* or MIRI LRS to detect with $\langle \text{S/N} \rangle \sim 5$. The added benefit of making this costly observation with MIRI LRS is that SO₂ could also be detected with $\langle \text{S/N} \rangle \sim 5$ from the 7.3 and 8.7 μm features. Nonetheless, detecting any gases other than CO₂ in a CO₂-dominated atmosphere will be very difficult.

4. Discussion

Our results indicate that *JWST* observations may be able to place strong constraints on the presence of high mean molecular weight terrestrial atmospheres for all of the TRAPPIST-1 planets and, in some cases, detect individual touchstone molecules that may be used to distinguish between different evolutionary histories that the planets may have undergone.

4.1. Do the TRAPPIST-1 Planets Have Atmospheres?

To detect the presence of atmospheres on the TRAPPIST-1 planets, we find that NIRSpec Prism observations are optimal. Transmission spectroscopy with NIRSpec Prism could lead to an $\langle \text{S/N} \rangle = 5$ detection of atmospheric spectral features in as few as 2–11 transits for TRAPPIST-1b out to TRAPPIST-1h if the planets lack high-altitude aerosols. However, if the TRAPPIST-1 planets possess Venus-like H₂SO₄ aerosols, reaching the same constraints on the presence of atmospheres may require up to 12 times more transits. CO₂ possesses numerous strong absorption bands from the near- through the mid-IR, such as the 2.0, 2.7, 4.2, and 15 μm bands, which significantly contribute to the ability of *JWST* to detect the terrestrial atmospheres considered in this work.

Our self-consistent Venus-like H₂SO₄ aerosol modeling reveals trends in the detectability of such atmospheres with semimajor axis. Lincowski et al. (2018) found that TRAPPIST-1b was too hot for Venus-like aerosols to form in the atmosphere, but that H₂SO₄ aerosols could form in all six exterior planets. These aerosols form at high altitudes in the atmospheres of TRAPPIST-1c, d, and e and lead to muted CO₂ features that will require about 4–12 times more transits to be detected with *JWST*. However, TRAPPIST-1f, g, and h are cool enough for the H₂SO₄ aerosols to form at lower altitudes (Lincowski et al. 2018), and therefore contribute less to their observable transmission spectra such that their atmospheres may be detected in fewer than two times the number of transits compared to the clear-sky CO₂ cases for the same planets. Cloudy Venus-like atmospheres for TRAPPIST-1f, g, and h require fewer transits to detect than cloudy Venus-like atmospheres for TRAPPIST-1c, d, and e.

Secondary eclipse spectroscopy may require a significantly greater *JWST* time commitment than transmission spectroscopy to achieve comparable constraints on the detection of the TRAPPIST-1 planet atmospheres. Because of its access to longer wavelengths, MIRI LRS is the only *JWST* instrument capable of observing eclipse spectra of the TRAPPIST-1 planets with high enough S/N to detect absorption features in the spectra that we considered. However, our estimates for the

JWST observing time required to detect emission spectrum features with MIRI LRS dwarfed the time required for spectral features to be detected in transmission spectra with NIRSpec, NIRISS, and NIRCam (see Figures 6, 13–19). Furthermore, the disparity between transmission and emission spectroscopy only broadens with semimajor axis, making precise MIRI LRS emission spectroscopy beyond TRAPPIST-1c infeasible with *JWST*. Our self-consistent planet models reveal that atmospheres with high-altitude aerosols—that may appear featureless in a transmission spectrum—may also appear featureless in an emission spectrum as thermal flux is emitted and/or scattered from near the top of the cloud deck.

Initial photometric assessments of the TRAPPIST-1 system with MIRI filter photometry are unlikely to provide more efficient preliminary results than transmission spectroscopy in the NIR with NIRSpec, NIRISS, or NIRCam. Our MIRI transit and eclipse photometry modeling showed that detecting the presence of atmospheres would require approximately an order of magnitude more *JWST* time than NIRSpec Prism transmission spectroscopy. This is due to (1) the higher S/N on transits afforded to NIRSpec near the peak of the stellar SED in the 1–3 μm range, (2) the usefulness of spectral resolution for atmospheric detections via deviations from a featureless spectrum, and (3) the need to observe transits in each MIRI filter separately to gain any meaningful wavelength resolution.

However, targeted MIRI photometric observations may still provide useful atmospheric constraints. Detecting the presence of atmospheric greenhouse heating may be done by inferring brightness temperatures that exceed the zero bond albedo equilibrium temperature. However, this will depend on the accuracy of MIRI’s absolute flux measurements. Specific wavelength bands where the observed atmosphere is optically thin, and therefore emits from hotter depths, provide the key observable. However, these observations may only be feasible for TRAPPIST-1b and c due to their higher expected thermal emission. The 11.3 μm MIRI filter (F1130W) may be optimal for such measurements because it is sufficiently separated from the strongly absorbing 15 μm CO₂ band. The 5.6 μm MIRI filter (F560W) may also be optimal for detecting high thermal emission from TRAPPIST-1b and c, if saturation on the star can be avoided in this bandpass. Transit and/or eclipse photometry targeting the 15 μm CO₂ band with the F1500W MIRI filter, and neighboring filters, could be used to detect the atmosphere, but our work shows that targeting the strong 4.2 μm CO₂ feature with NIRSpec Prism transmission spectroscopy will be a much more efficient approach for detecting CO₂ in an atmosphere.

Detecting wavelength-dependent surface emissivity features in the emission spectrum of a planet without an atmosphere will be highly unlikely with *JWST*. Even for the optimistic case—TRAPPIST-1b with a pure and smooth quartz surface—we find it would require \sim 90 secondary eclipses with MIRI LRS to detect the mid-IR silicate absorption (see Figure 11). Consequently, detecting surface features on an airless world would be extremely challenging. This validates our assumption that an airless planet will likely appear featureless in emission, and that detecting spectral features due to surface emissivity variations is an inefficient means to confirm that a planet is airless. Furthermore, this strengthens the case for transmission spectroscopy, which can detect the high mean molecular weight atmosphere of a Venus-like planet enshrouded in H₂SO₄ clouds in just \sim 20–30 transits (for TRAPPIST-1c, d, and e). However, actually confirming that a TRAPPIST-1

planet does not possess an atmosphere—even if featureless spectra favor that hypothesis—will be a very difficult task that may require observations of thermal phase curves (Selsis et al. 2011; Maurin et al. 2012; Kreidberg & Loeb 2016; Meadows et al. 2018) or planet–planet occultations (Luger et al. 2017a) to probe the day–night temperature contrast.

Comparison with Previous Works—Our results are in agreement with previous investigations on optimal ways to detect terrestrial exoplanet atmospheres of different compositions. Although emission spectroscopy has been suggested as a means of detecting terrestrial atmospheres (e.g., Belu et al. 2011), we agree with previous works that transmission spectroscopy is more viable (e.g., Hedelt et al. 2013; Barstow & Irwin 2016; Barstow et al. 2016; Greene et al. 2016), particularly for temperate and cool planets that emit considerably less thermal flux. We agree with Bétrémeix & Swain (2018) that the *JWST* integration times needed to detect molecules strongly depend on the composition of the atmosphere—particularly the presence of high-altitude aerosols.

Although we considered more atmospheric compositions, our predicted exposure times for the detection of planetary atmospheres agree for the subset of similar atmospheres modeled by Morley et al. (2017), with many of the discrepancies attributable to differences in the assumed planetary masses used in the transmission spectrum models. Our work and that of Morley et al. (2017) have a common focus of distinguishing clear-sky Venus-like atmospheres from a featureless spectrum with the NIRSpec/G235 instrument, which offers a basis for comparison. The detectability of these atmospheres is dominated by CO₂ features, which are largely unaffected by photochemistry, which was not included in Morley et al. (2017). We find that a 10 bar CO₂ atmosphere would require 5, 8, 4, 17, 15, 16, and 15 transits to distinguish TRAPPIST-1b, c, d, e, f, g, and h, respectively, from a featureless spectrum, and Morley et al. (2017) found that a 1 bar aerosol-free Venus-like atmosphere would require 6, 36, 13, 4, 17, 10, and 4 transits.

The cases of largest disagreement (e.g., c, e, h) appear consistent with the different masses used in each study. Planet mass affects the atmospheric scale height (via the surface gravity) and therefore the size and detectability of molecular features in a transmission spectrum. Morley et al. (2017) used masses from Wang et al. (2017), with the exception of TRAPPIST-1f, for which the mass from Gillon et al. (2017) was used. In this paper, and in Lincowski et al. (2018), we use the TRAPPIST-1 planet masses from Grimm et al. (2018). For the case of TRAPPIST-1c, where we use a significantly smaller planet mass than Morley et al. (2017), we find that fewer transits are required to detect spectral features in transit. For the cases of TRAPPIST-1e and h, where we use a significantly larger planet mass than Morley et al. (2017), we find that more transits are required to detect spectral features. This scaling with mass is consistent with the findings of Morley et al. (2017) when they repeated calculations with masses derived from the Weiss & Marcy (2014) mass–radius relationship, and further underscores the need for accurate masses for spectral modeling and fitting.

Our focus on thicker atmospheres (1–100 bar) than those in Morley et al. (2017; 0.01–1 bar) both explains discrepancies between the studies and further demonstrates that such thick and aerosol-free atmospheres may be more easily detected than thinner atmospheres. Our results for TRAPPIST-1d, where our masses agree best, show nine fewer transits required to detect spectral features than Morley et al. (2017), which is consistent with the different planet surface pressures used in each study. Morley et al. (2017) demonstrated a trend of increasing

atmospheric detectability with increasing surface pressure in simulations of 0.01, 0.1, and 1 bar CO₂ atmospheres. Our results continue this nearly linear trend in log-pressure out to 10 bars. However, our 92 bar CO₂ atmospheres are consistent with the detectability of our 10 bar atmospheres, indicating that this trend in pressure saturates for thick atmospheres as the planet surface drops below the atmospheric regions that are sensed with transmission spectroscopy.

The Krissansen-Totton et al. (2018) work on the detectability of biogenic gases in an anoxic atmosphere for TRAPPIST-1e with *JWST* suggests that relatively few transits are required to constrain atmospheric abundances. Krissansen-Totton et al. (2018) showed that a retrieval using \sim 10 transits of TRAPPIST-1e with NIRSpec Prism was sufficient to begin to constrain the abundances of CO, CO₂, and CH₄. Consequently, the 13 transits of TRAPPIST-1e that we show may be required to detect a clear 1 bar H₂O atmosphere to $\langle S/N \rangle = 5$, may also provide spectra that are sufficient to begin to constrain molecular abundances in an atmospheric retrieval framework.

HST transmission spectroscopy of hot gaseous exoplanets has demonstrated how the presence of clouds and hazes can diminish sensitivity to molecular absorption features (e.g., Berta et al. 2012; Ehrenreich et al. 2014; Knutson et al. 2014; Kreidberg et al. 2014; Nikolov et al. 2015; Sing et al. 2016), but we know a priori that planets with such large radii must have atmospheres. However, for terrestrials, we will rely on absorption features to test for the presence of atmospheres, and clouds and hazes, if present, will make this more difficult. Batalha et al. (2018) concluded that 10 transits should be sufficient to detect the dominant molecular absorber in the transmission spectrum of TRAPPIST-1f when observed using a partial saturation strategy with NIRSpec Prism, and that additional observations are unlikely to reveal more information. While our results agree with Batalha et al. (2018) for the case of clear atmospheres, cloudy and/or hazy terrestrial atmospheres may require significantly more observations. Venus-like planets with H₂SO₄ aerosols tend to require more than 10 transits (and up to \sim 30 for TRAPPIST-1e) to reach the same confidence in the detection of the atmosphere. We recommend testing the hypothesis that a TRAPPIST-1 (or similar) planet has a clear atmosphere in ≤ 10 transits, and then evaluating the scientific value of additional transits to test the hypothesis that the planet has aerosols.

4.2. What is the Nature of the TRAPPIST-1 Planet Atmospheres?

Detecting specific molecules in *JWST* transmission spectra of the TRAPPIST-1 planets may be possible and allow for discrimination among different climate/composition states and evolutionary histories. As previously stated, CO₂ should be the easiest molecule for *JWST* to detect in the atmospheres of the TRAPPIST-1 planets. Due to its prevalence in these simulated atmospheres regardless of evolutionary history, CO₂ makes for a strong indicator of a terrestrial atmosphere, but a weak discriminant of specific atmospheric state. Furthermore, CO₂ produces nearly the same strength features regardless of atmospheric abundance, particularly the 4.3 and 15 μm bands, which are saturated in a Venus-like atmosphere, an O₂ outgassing atmosphere, and an Earth-like atmosphere, even though the abundance ranges from 90 bars down to 360 ppm (Lincowski et al. 2018). Other molecules, such as O₂, O₃, H₂O, and SO₂, may be detectable with *JWST* and may help to distinguish among the suite of atmospheres that we considered.

Although oxygen as a biosignature may not be detectable for the potentially habitable TRAPPIST-1 planets, oxygen as a remnant of pre-main-sequence water loss may be easily detected or ruled out. We find that biogenic O₂ in the atmosphere of TRAPPIST-1e may be too difficult to detect with *JWST*, but the 9.6 μm O₃ feature may be weakly detectable at $\langle S/N \rangle = 3$ in over 100 transits with MIRI LRS, which is in general agreement with the findings of Wunderlich et al. (2019). However, the 1.06 and 1.27 μm O₂-O₂ CIA features are key discriminants of a planet that has an oxygen abundance greatly exceeding biogenic oxygen production on Earth and may therefore indicate a planet that has undergone vigorous water photolysis and subsequent loss during the protracted super-luminous pre-main-sequence phase faced by late M dwarfs (Luger & Barnes 2015; Schwertner et al. 2016). We find that NIRSpec G140M/H is the optimal *JWST* instrument for detecting these O₂-O₂ features and could lead to their detection in as few as 7–9, 15, 8, 49–67, 55–82, 79–100, and 62–89 transits of TRAPPIST-1b, c, d, e, f, g, and h, respectively, should they possess such an atmosphere. These quoted number of transits may be sufficient to rule out the existence of oxygen-dominated atmospheres in the TRAPPIST-1 system. Additional evidence of ocean loss could be provided by detection of isotope fractionation, which may also be possible in as few as 11 transits with *JWST*, for strong isotopologue bands such as HDO (Lincowski et al. 2019).

Detecting ozone absorption may be another strong indicator of a post-runaway, oxygen-dominated atmosphere. For the 10 bar desiccated O₂ atmospheres, ozone absorption features become more detectable for the outer planets. Targeting O₃ at 9.6 μm with MIRI LRS is optimal for the inner planets (b, c, d, e), although it may require upwards of 100 transits to detect at $\langle S/N \rangle = 5$. However, targeting the weaker O₃ bands between 3 and 5 μm with NIRSpec G395M/H or NIRSpec Prism is optimal for the outer planets (f, g, h), due to their larger ozone column abundances. The O₂-O₂ CIA bands for these cooler, desiccated planets are more difficult to detect, which may make O₃ a more efficient observational discriminant for such a planet.

The photochemistry underlying the detectable ozone buildup in the cooler planets has implications beyond the TRAPPIST-1 system. Lincowski et al. (2018) noted that the competing effects of the Chapman cycle (with declining photolysis rates with distance from the star), was primarily responsible for the ozone accumulation in the atmospheres of the outer planets, an effect previously noticed by Grenfell et al. (2007). While this is a driving factor, the differences among the planets can more specifically be attributed to catalytic cycles of nitrogen oxides (primarily, N₂O, NO, and NO₂), which drive the destruction of O₃, as in the stratosphere of Earth (Seinfeld & Pandis 2006). Because these atmospheres contain N₂, O¹D produced from photolysis of oxygen-bearing molecules can react with N₂ to generate nitrogen oxides. The availability of O¹D declines with distance from the star due to lower UV fluxes. Beginning with planet e, the production of nitrogen oxides declines substantially, removing them as a mechanism for the destruction of O₃, so that O₃ accumulates and becomes well-mixed, generating a large column density. In the atmosphere of an O₂-dominated atmosphere without N₂, O₃ levels would likely be higher, due to the lack of the nitrogen oxide catalysts.

Detecting water in the atmospheres of the TRAPPIST-1 planets may also help to constrain evolutionary scenarios. The presence of water may be readily detectable for TRAPPIST-1b, c, and d with NIRSpec Prism* if they possess high O₂

atmospheres that have not been completely desiccated. High O₂ atmospheres for planets that exited the pre-main sequence with their atmospheres and interiors completely desiccated, however, will have no water to detect, making water in an oxygen-dominated atmosphere a potentially detectable discriminant of incomplete desiccation or outgassing from the interior. In CO₂-dominated atmospheres, H₂O may be prohibitively difficult to detect, due to its scarcity in the atmospheres of Venus-like worlds, before even considering obscuration by H₂SO₄ clouds.

Detecting water in the atmosphere of one of the potentially habitable TRAPPIST-1 planets could indirectly hint at surface habitability (Robinson 2018), but this will be challenging for *JWST*, even with an ideal system like TRAPPIST-1. Tropospheric H₂O may be detectable in the transmission spectrum of TRAPPIST-1e in \sim 35 transits with NIRSpec Prism* should the planet have a clear-sky 1 bar N₂/O₂ atmosphere with H₂O. However, the cold trap that keeps water vapor concentrated in the lower atmosphere makes habitability difficult to infer with transmission spectroscopy, which cannot readily probe surface environments. Additionally, we find that 100% cloud coverage strongly increases the required *JWST* time to detect H₂O in such a habitable atmosphere. Given these difficulties for detecting water in the atmosphere of a habitable-zone planet with *JWST*, robust habitability assessments may ultimately require a future direct imaging telescope that can readily probe rocky planet surfaces to search for more direct evidence of surface liquid water (e.g., Cowan et al. 2009; Robinson et al. 2010; Lustig-Yaeger et al. 2018).

4.3. Further Considerations

The results in this paper lean optimistic, and therefore represent lower limits on the amount of observing time needed to detect and characterize evolved terrestrial atmospheres in the TRAPPIST-1 system. As a result, TRAPPIST-1 observing plans that include fewer transits/eclipses than reported here may require additional observations to make robust inferences on the existence and nature of atmospheres. One source of optimism is that our $\langle S/N \rangle$ approach (see Equation (6)) to atmospheric and molecular detection, rather than a full atmospheric retrieval, implicitly assumes that any retrieval will have converged on the true underlying spectrum. As a result, our S/N metric is not equal to a detection of that specific atmosphere to a given significance (e.g., 3σ). In practice, many different atmospheric compositions will likely be capable of fitting *JWST* spectra of TRAPPIST-1 planets, potentially leaving large regions of atmospheric parameter space unconstrained. Thus, the confidence of any “one” composition representing the true state of the planet may remain low despite having high confidence in the presence of features in the spectrum that would indicate the presence of an atmosphere. Our approach is simply a wavelength-range- and resolution-agnostic method to quantify the detectability of spectral signals emanating from self-consistent atmospheres above the expected noise of *JWST*.

Our calculations also lean optimistic because we have ignored astrophysical and systematic sources of noise that may make precise time-series exoplanet observations with *JWST* more difficult than our estimates suggest. Stellar effects such as limb darkening (e.g., Csizmadia et al. 2013) and heterogeneous photospheres (e.g., Rackham et al. 2017, 2018; Zhang et al. 2018) are major concerns for precision exoplanet transmission spectroscopy. These effects may be particularly perilous for observations of planets orbiting low-mass stars, as the stars may contain large, cool spots and

absorbing molecules in their photospheres. We also did not assume a systematic noise floor for any *JWST* instruments (e.g., Greene et al. 2016), but this is likely optimistic in terms of the currently unknown on-target performance. Astrophysical and systematic effects must be well understood to detect molecular features at the \sim 10 ppm level, where many terrestrial features reside. However, many of the major absorption features in our TRAPPIST-1 planet spectral models are much larger and more detectable, spanning 50–200 ppm.

During the preparation of this paper, a new version of *Pandelia* was released (version 1.3) that increased *JWST* background noise predictions by 10–40 ppm. For bright targets like TRAPPIST-1, where the noise budget is dominated by stellar photon noise, such an increase in the background has a negligible effect on our estimated number of transits and eclipses to detect and characterize exoplanet atmospheres in the near- through the mid-IR.

We considered a limited number of atmospheres that may not resemble the true state of the TRAPPIST-1 planets, especially because the star’s UV spectrum is poorly constrained. Here, as in Lincowski et al. (2018), we used a UV spectrum scaled from measurements of the nearby mid M dwarf Proxima Centauri, but these stars have slightly different spectral types and activity levels. Recently, three synthetic SEDs have been produced by Peacock et al. (2019) for TRAPPIST-1, which are constrained by the Ly α flux and upper limits of *Galaxy Evolution Explorer* UV photometry. These synthetic spectra differ by having higher NUV and a different distribution of far-UV flux than Lincowski et al. (2018), which could slightly change the photochemistry of these planetary atmospheres and the observable molecular absorption in their upper atmospheres. However, only observations—including those outlined in this paper—will ultimately reveal what planetary processes dominate in sculpting the observable atmospheric signatures of terrestrial exoplanets, particularly those orbiting M dwarfs. In the mean time, further study is warranted on the range of possible atmospheric conditions for the TRAPPIST-1 planets, particularly photochemically and climatically self-consistent reducing atmospheres (e.g., Arney et al. 2017), and UV characterizations of late M dwarfs to improve photochemical predictions and interpretation of observations.

Although the atmospheric states considered in this paper represent only a selection of possible states, many of their characteristics and molecular features may exist in other atmospheres, making our results apply more broadly. For example, the strength of the H₂O, CO₂, and O₃ bands in the O₂-dominated outgassing atmospheres may be similar in other clear atmospheres that may contain more inert gases, like N₂. Our *JWST* detectability calculations for these gases may be useful beyond that particular atmospheric case. The O₂-O₂ features, however, are specific evidence of high O₂ content. Because all of the atmospheres considered in this work were high mean molecular weight, our results help to elucidate the detectability of such atmospheres and the molecules within, even if the true compositions differ.

Constraining the atmospheres of Earth-size planets transiting even the smallest stars like TRAPPIST-1 will require pushing the limits of *JWST*. As we demonstrated with the NIRSpec Prism partial saturation, alternate *JWST* modes that can improve observations of transiting exoplanets can enhance the science return, and dramatically decrease the time investment required to detect and characterize terrestrial atmospheres. Although modes such as NIRCam’s Dispersed

Hartmann Sensor (Schlawin et al. 2017) and high-efficiency readout patterns for NIRSpec Prism (Batalha et al. 2018) have not been officially approved, they represent promising avenues toward improved *JWST* observations that may ultimately make the difference in enabling *JWST* to constrain terrestrial exoplanet atmospheric compositions.

5. Conclusion

We investigated the potential to detect and characterize the atmospheres of all seven known TRAPPIST-1 exoplanets with *JWST*. Although the planets are small and likely possess high mean molecular weight atmospheres with relatively low scale heights, we found that many molecular absorption features may be detectable with *JWST* in $\sim 2\text{--}15$ transits. These observations may be used to diagnose the presence of atmospheres and, in some cases, discriminate between different plausible atmospheric compositions.

However, we find that an initial photometric assessment of the TRAPPIST-1 planets with MIRI is, perhaps non-intuitively, not as efficient as spectroscopic atmosphere detection in the NIR. To achieve comparable constraints on the detection of atmospheres, approximately an order of magnitude more transits or eclipses will need to be observed with MIRI, compared to transits observed with spectrometers in the NIR.

Transmission spectroscopy with NIRSpec Prism may be the most efficient path to detect the presence of atmospheres for the TRAPPIST-1 planets, via detecting CO₂ bands between 1 and 5 μm . Venus-like atmospheres with high-altitude H₂SO₄ aerosols will be more difficult to detect in transmission and emission spectra, however, these aerosols will form at lower altitudes for the temperate and cooler planets such that they obscure less molecular absorption in transmission spectra. Furthermore, post-runaway oxygen-dominated worlds may be identified in transmission using (1) O₂–O₂ CIA observed with NIRSpec G140M/H, NIRSpec Prism, or NIRISS SOSS, or (2) O₃ absorption observed with MIRI LRS (for b, c, d, and e) or NIRSpec G395M/H (for f, g, and h). If TRAPPIST-1e is habitable and cloud-free, water could be detected in the troposphere with NIRSpec Prism in about 35 transits, but the presence of water clouds could completely obscure the water vapor absorption features.

We outlined a particular path for characterizing the TRAPPIST-1 planets with *JWST* that narrows down the possible evolutionary histories that the planets may have had to exist in their current observable states. We recommend using transmission spectroscopy to

1. detect the planet atmospheres via CO₂ absorption,
2. detect or rule out post-runaway oxygen-dominated atmospheres via O₂–O₂ CIA or O₃ absorption, and
3. constrain the extent of (atmosphere and interior) desiccation, and potentially the habitability, via the H₂O abundance.

However, our results may be used to construct countless additional observing strategies that best augment existing projects and proposals with our testable hypotheses on the nature of TRAPPIST-1 system of Earth-sized exoplanets.

We thank Eric Agol for insights into our photometric signal-to-noise calculations, Joshua Bandfield and Elena Amador for crucial discussions on the emissivity signatures of rocks, and Rodrigo Luger for countless useful discussions that contributed to this

work. We also thank the anonymous referee whose helpful comments contributed to the quality and clarity of this paper. This work was performed as part of NASA’s Virtual Planetary Laboratory, supported by the National Aeronautics and Space Administration through the NASA Astrobiology Institute under solicitation NNH12ZDA002C and Cooperative Agreement Number NNA13AA93A, and by the NASA Astrobiology Program under grant 80NSSC18K0829 as part of the Nexus for Exoplanet System Science (NExSS) research coordination network. This work made use of the advanced computational, storage, and networking infrastructure provided by the Hyak supercomputer system at the University of Washington.

Software: Astropy (Astropy Collaboration et al. 2013; Price-Whelan et al. 2018), Matplotlib (Hunter 2007), Numpy (van der Walt et al. 2011), SMART (Meadows & Crisp 1996), Pandexia (Pontoppidan et al. 2016), PandExo (Batalha et al. 2017, 2018), pysynphot (STScI Development Team 2013).

Appendix A S/N on Transit and Eclipse Depths

Transit and eclipse depth measurements are both relative to the out-of-occultation measurement, and thus require accounting for photon fluence in and out of the event of interest. Below we derive the S/N on measurements of transit and eclipse depths by considering the signal as the occultation depth, which must be calculated from the difference between in- and out-of-event observations, and the noise by propagating individual measurement errors through the signal calculation.

For the primary transit, the signal of interest is the number of photons missing when the star is occulted by the planet. Ignoring photons emitted and reflected by the planet prior to and during transit, the out-of-transit photon fluence is measured as

$$N_{\text{out}} = (N_s + N_{bg})n_{\text{out}}, \quad (11)$$

where n_{out} is the time of measurement outside of transit in units of the transit duration, and N_s and N_{bg} are the total number of photons counted over a transit duration. The in-transit photon fluence measured is

$$N_{tr} = N_s \left(1 - \left(\frac{R_p}{R_s} \right)^2 \right) + N_{bg}. \quad (12)$$

The number of stellar photons blocked by the planet can be estimated from

$$N_{sp} = N_{\text{out}}/n_{\text{out}} - N_{tr}; \quad (13)$$

this is the signal we seek to measure. The noise on N_{sp} can be calculated by considering the variance given standard uncorrelated error propagation:

$$\sigma^2 = \left(\frac{\partial N_{sp}}{\partial N_{\text{out}}} \right)^2 \sigma N_{\text{out}}^2 + \left(\frac{\partial N_{sp}}{\partial N_{tr}} \right)^2 \sigma N_{tr}^2 \quad (14)$$

$$= \left(\frac{1}{n_{\text{out}}} \right)^2 N_{\text{out}} + (-1)^2 N_{tr} \quad (15)$$

$$= \frac{(N_s + N_{bg})}{n_{\text{out}}} + N_s \left(1 - \left(\frac{R_p}{R_s} \right)^2 \right) + N_{bg}. \quad (16)$$

Finally, the S/N on the transit depth can be constructed by dividing the blocked photons N_{sp} by the standard deviation on

that estimate:

$$S/N_T = \frac{N_s(R_p/R_s)^2}{\sqrt{(N_s + N_{bg})/n_{out} + N_s(1 - (R_p/R_s)^2) + N_{bg}}}. \quad (17)$$

For the secondary eclipse, the signal of interest is the number of photons missing when the planet is occulted by the star, which is measured assuming that the star is not varying. In this case, the out-of-eclipse photon fluence is measured as

$$N_{out} = (N_p + N_s + N_{bg})n_{out}, \quad (18)$$

where n_{out} is the time of measurement outside of the eclipse in units of the eclipse duration, N_p is the total number of planet photons over an eclipse duration, and the sum of N_p , N_s , and N_{bg} is the total number of photons counted over an eclipse duration. The in-eclipse photon fluence measured is

$$N_{ec} = N_s + N_{bg}, \quad (19)$$

which allows the planet photon counts to be estimated as

$$N_p = N_{out}/n_{out} - N_{ec}. \quad (20)$$

Again, analogous to the transit calculation, the noise term can be calculated by considering the variance on N_p given standard error propagation:

$$\sigma^2 = \left(\frac{\partial N_p}{\partial N_{out}} \right)^2 \sigma N_{out}^2 + \left(\frac{\partial N_p}{\partial N_{ec}} \right)^2 \sigma N_{ec}^2 \quad (21)$$

where we have used the fact that N_{out} has a variance of N_{out} . Substituting in for N_{out} and N_{ec} gives

$$\sigma^2 = \frac{(N_p + N_s + N_{bg})}{n_{out}} + N_s + N_{bg}. \quad (23)$$

Finally, the S/N on the eclipse depth can be constructed by dividing the estimated planet photons by the standard deviation on that estimate:

$$S/N_E = \frac{N_p}{\sqrt{(N_p + N_s + N_{bg})/n_{out} + N_s + N_{bg}}}. \quad (24)$$

Appendix B Atmospheric Detectability by Instrument

Figures 13–19 show the number of transits needed to detect the atmospheres of TRAPPIST-1b, c, d, e, f, g, and h, respectively, as a function of both atmospheric compositions and *JWST* instrument/mode. We adopt the assumption that the detection of an atmosphere requires $\langle S/N \rangle = 5$ on spectral features in the transmission spectrum.

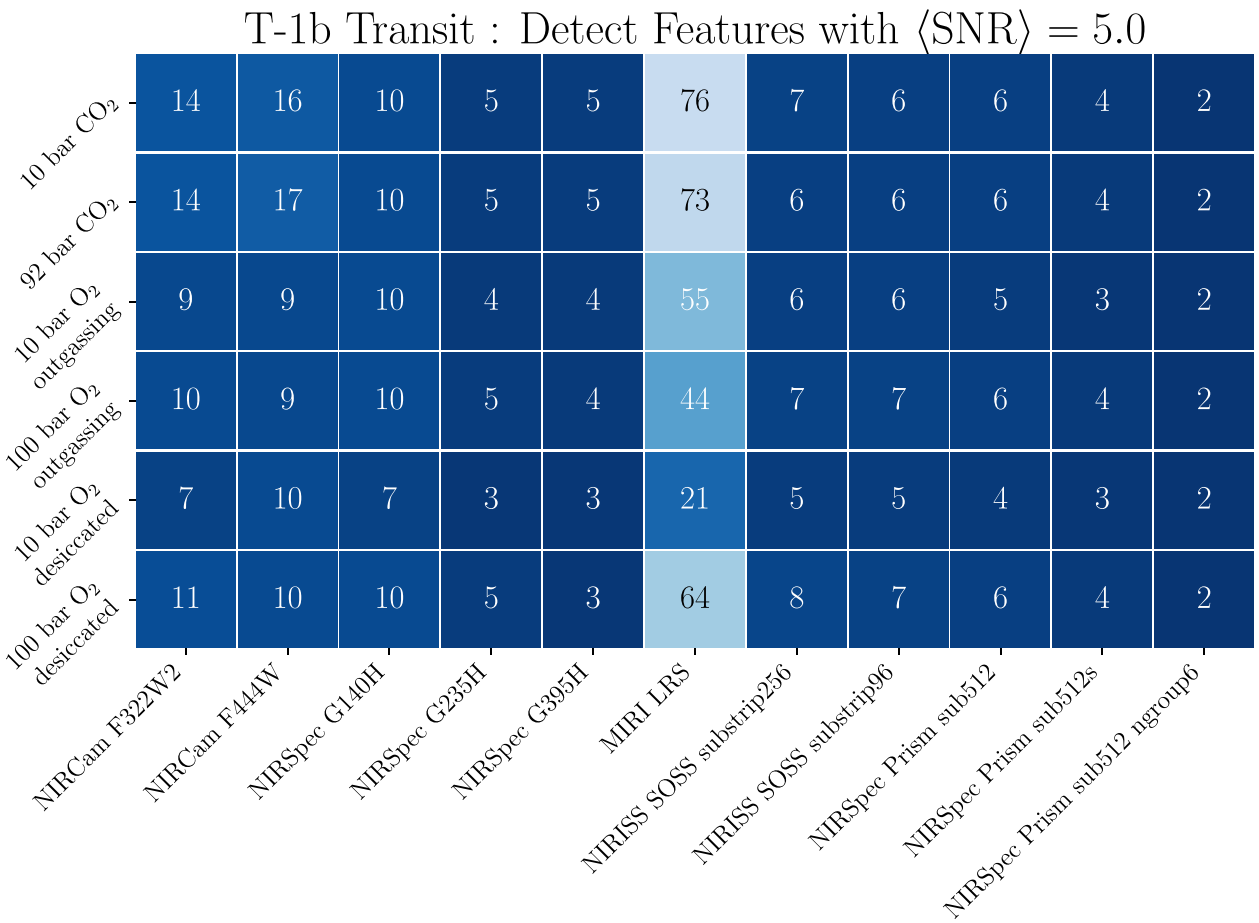


Figure 13. Number of TRAPPIST-1b transits necessary to rule out a featureless spectrum with $\langle S/N \rangle = 5$ for different atmospheric compositions and using different *JWST* instruments and modes.

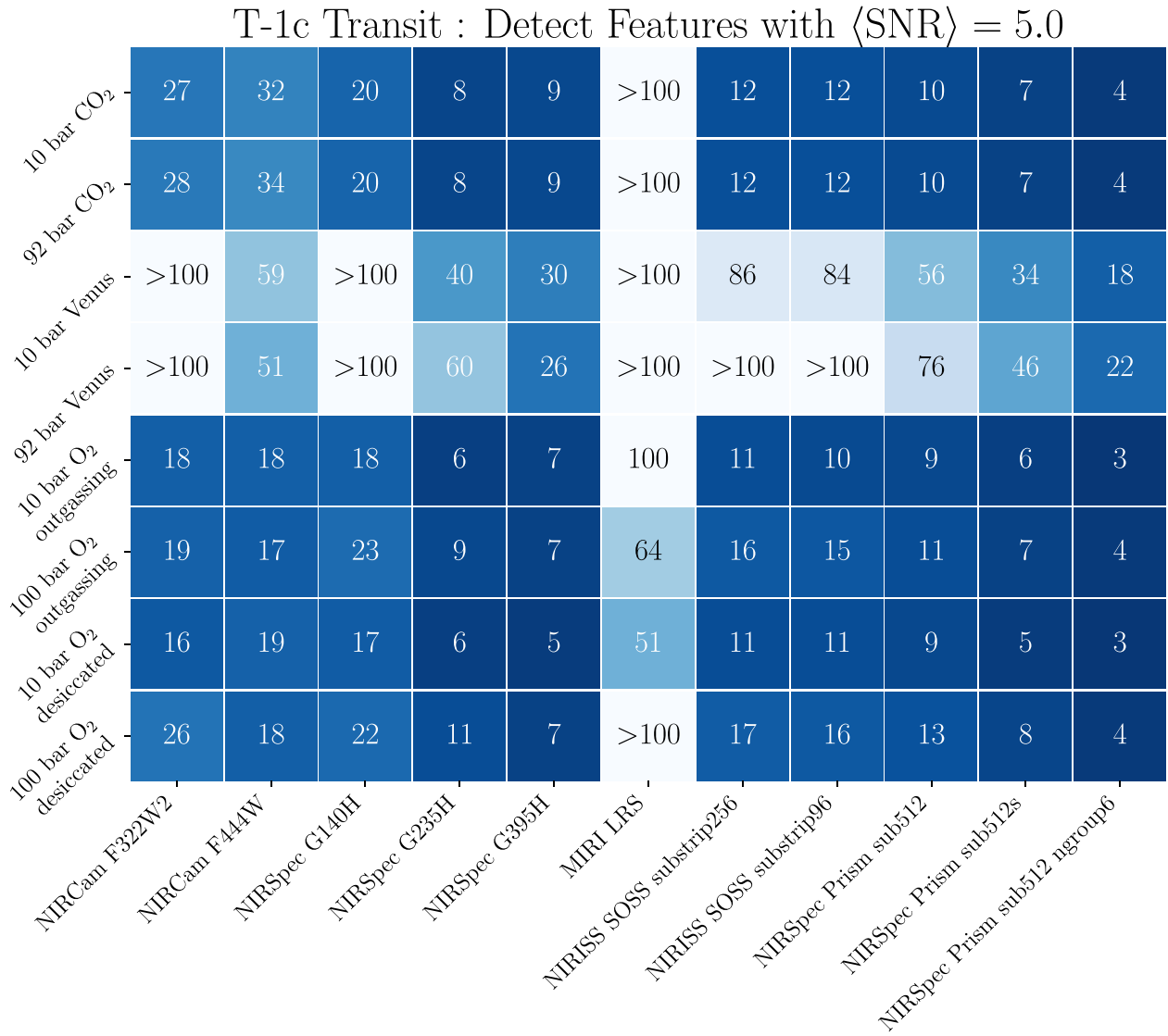


Figure 14. Number of TRAPPIST-1c transits necessary to rule out a featureless spectrum with $\langle \text{S/N} \rangle = 5$ for different atmospheric compositions and using different *JWST* instruments and modes.

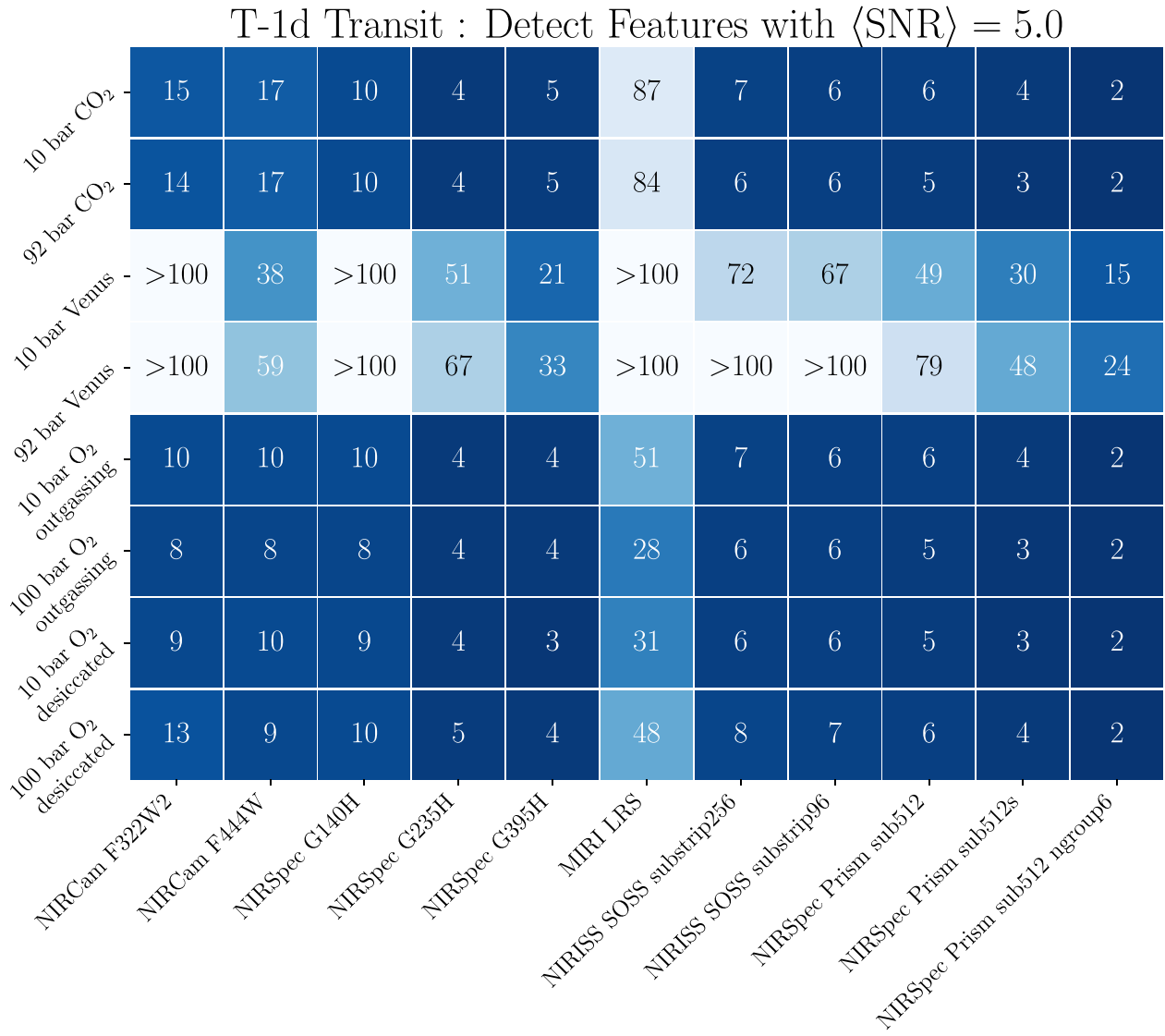


Figure 15. Number of TRAPPIST-1d transits necessary to rule out a featureless spectrum with $\langle \text{S/N} \rangle = 5$ for different atmospheric compositions and using different *JWST* instruments and modes.

T-1e Transit : Detect Features with $\langle \text{SNR} \rangle = 5.0$

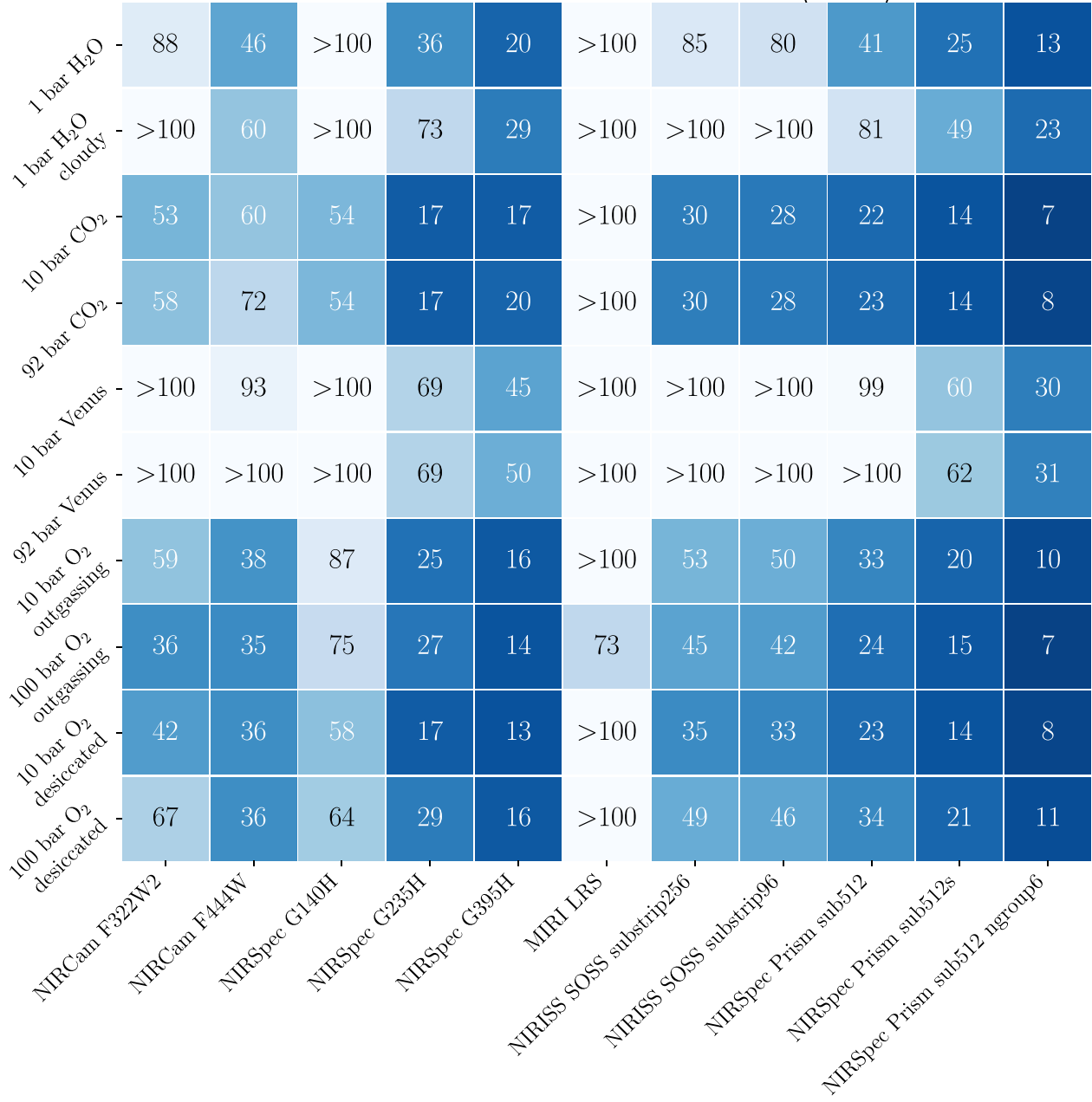


Figure 16. Number of TRAPPIST-1e transits necessary to rule out a featureless spectrum with $\langle \text{S/N} \rangle = 5$ for different atmospheric compositions and using different *JWST* instruments and modes.

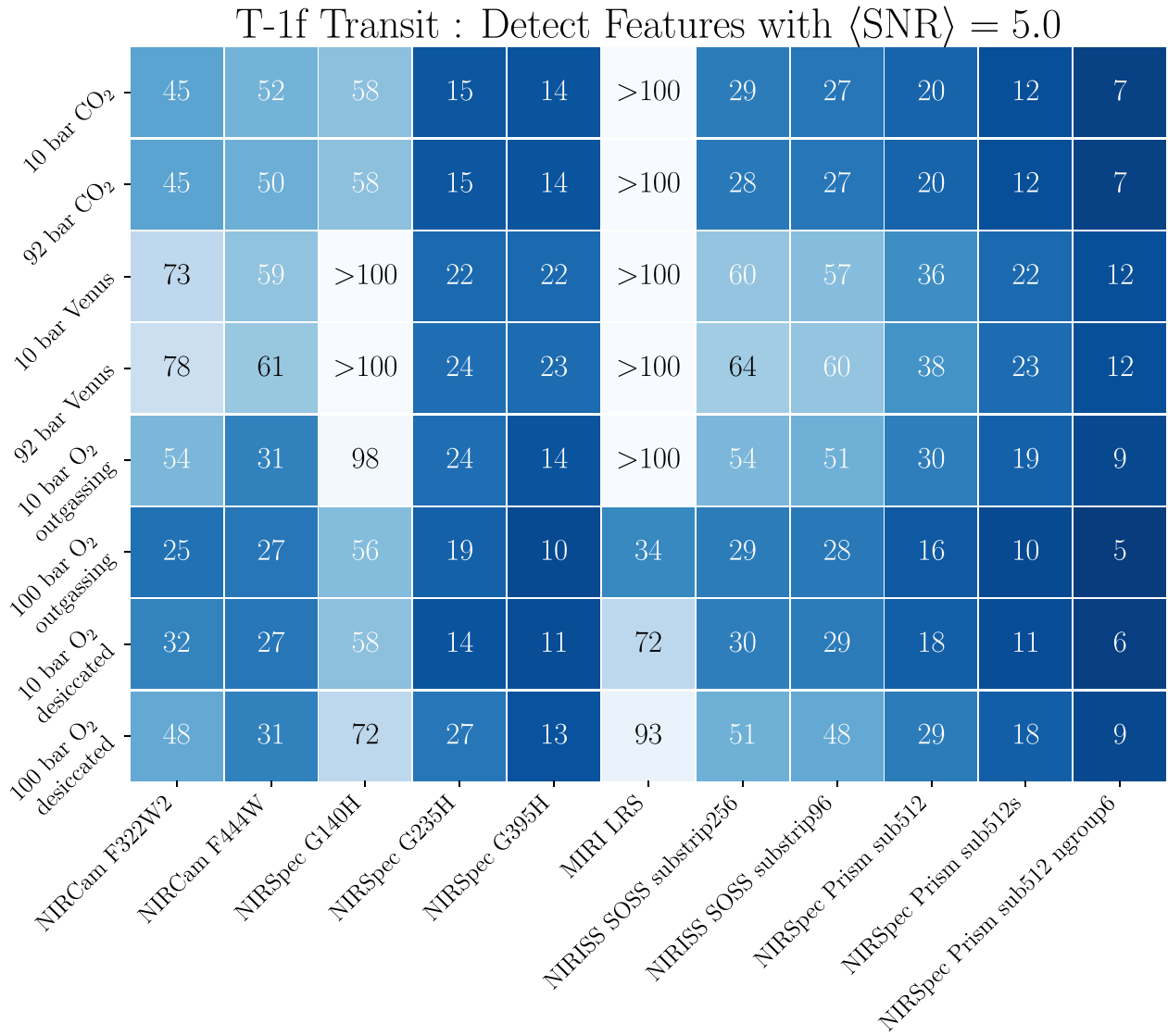


Figure 17. Number of TRAPPIST-1f transits necessary to rule out a featureless spectrum with $\langle \text{S/N} \rangle = 5$ for different atmospheric compositions and using different *JWST* instruments and modes.

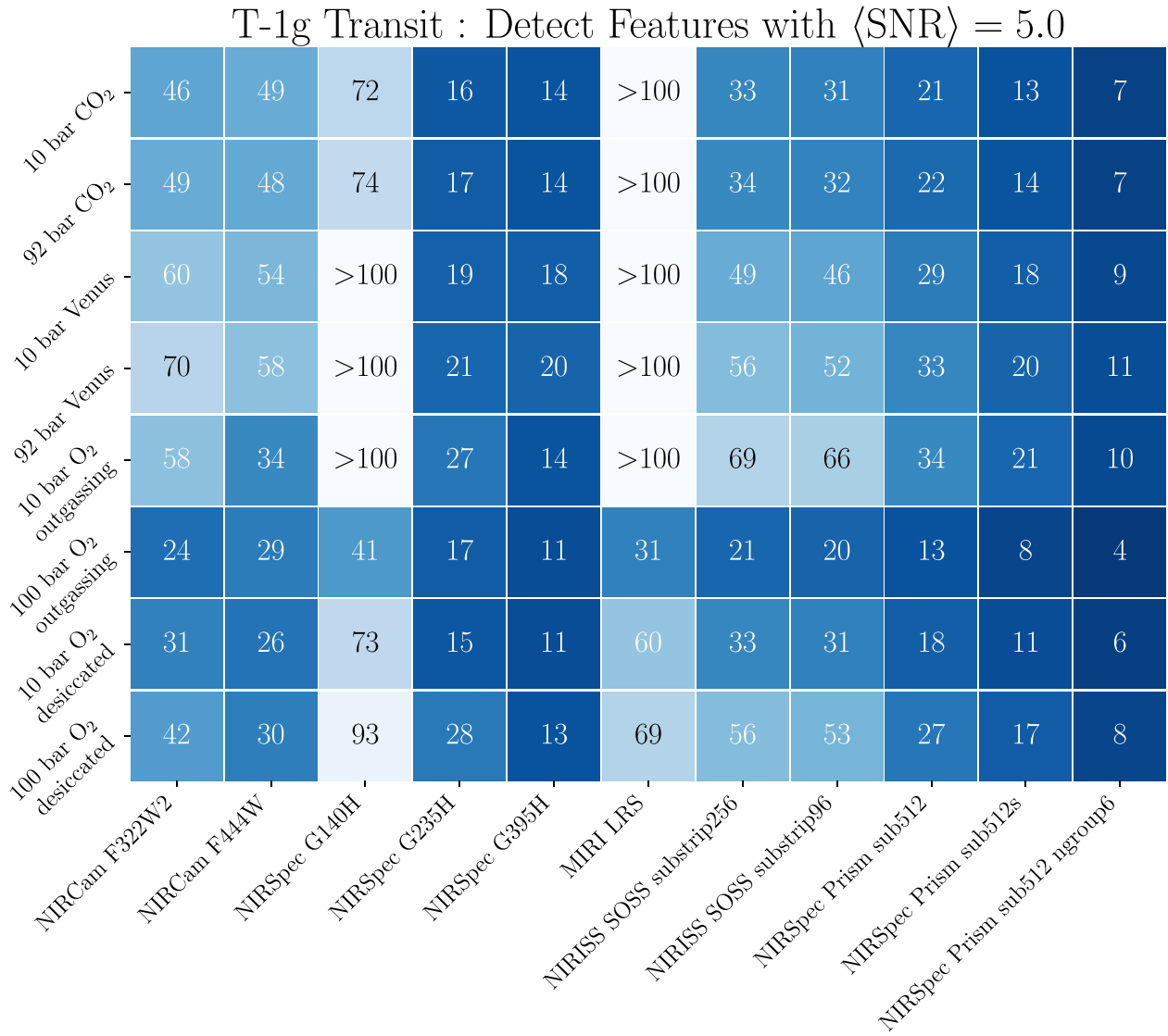


Figure 18. Number of TRAPPIST-1g transits necessary to rule out a featureless spectrum with $\langle \text{S/N} \rangle = 5$ for different atmospheric compositions and using different *JWST* instruments and modes.

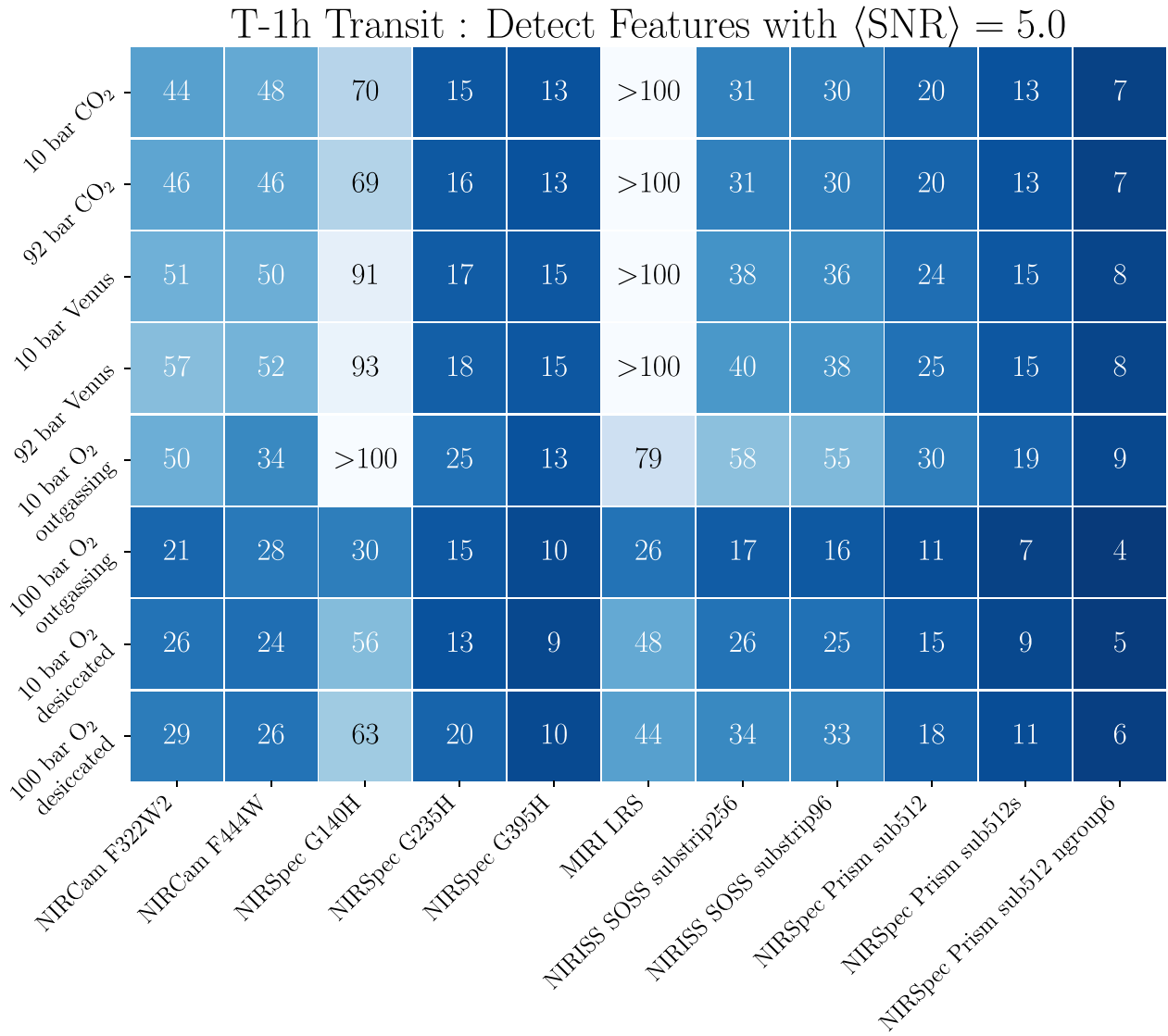


Figure 19. Number of TRAPPIST-1h transits necessary to rule out a featureless spectrum with $\langle \text{S/N} \rangle = 5$ for different atmospheric compositions and using different *JWST* instruments and modes.

Appendix C Brightness Temperatures

Table 3 shows the brightness temperature of each Lincowski et al. (2018) TRAPPIST-1 atmospheric model in each of the

JWST/MIRI photometric filters and the two warm *Spitzer* bands.

Table 3
Brightness Temperatures in Different Photometric Filters for Different Models

Planet	Model	IRAC1 (K)	IRAC2 (K)	F560W (K)	F770W (K)	F1000W (K)	F1130W (K)	F1280W (K)	F1500W (K)	F1800W (K)	F2100W (K)	F2550W (K)
T-1b	10 bar CO ₂	498	328	432	384	340	356	330	291	315	362	430
	92 bar CO ₂	495	328	432	383	340	357	330	289	315	362	430
	100 bar O ₂ outgassing	500	388	372	396	379	432	385	305	355	381	346
	10 bar O ₂ outgassing	514	391	357	394	394	425	377	300	345	371	329
	100 bar O ₂ desiccated	425	375	390	387	389	404	376	306	368	408	364
	10 bar O ₂ desiccated	436	357	401	405	369	397	360	292	346	408	380
	10 bar CO ₂	445	292	385	328	304	326	295	250	275	315	386
T-1c	92 bar CO ₂	437	290	380	324	303	326	293	248	273	313	382
	100 bar O ₂ outgassing	434	337	325	346	312	390	343	266	325	345	308
	10 bar O ₂ outgassing	424	334	313	350	337	378	330	252	304	332	294
	100 bar O ₂ desiccated	387	325	330	328	333	339	327	272	325	342	310
	10 bar O ₂ desiccated	395	313	339	341	322	345	318	257	310	347	322
	10 bar Venus	427	292	373	318	300	320	296	272	282	313	376
	92 bar Venus	435	287	382	317	297	324	291	250	275	303	383
T-1d	10 bar CO ₂	384	256	337	274	269	295	260	219	239	272	340
	92 bar CO ₂	380	254	333	271	268	295	259	215	237	269	337
	100 bar O ₂ outgassing	370	290	280	301	264	352	295	227	290	305	270
	10 bar O ₂ outgassing	361	283	270	299	287	324	285	215	267	291	260
	100 bar O ₂ desiccated	356	281	278	274	280	279	280	239	282	284	260
	10 bar O ₂ desiccated	362	275	286	286	279	293	277	225	275	292	269
	10 bar Venus	326	258	240	230	230	233	233	227	231	239	243
T-1e	92 bar Venus	375	251	332	264	263	288	256	223	245	271	335
	10 bar CO ₂	339	230	297	235	247	272	232	193	208	237	301
	92 bar CO ₂	335	226	292	229	243	267	228	189	206	233	294
	100 bar O ₂ outgassing	305	236	244	259	231	301	245	203	253	265	245
	10 bar O ₂ outgassing	346	243	243	256	243	267	244	191	239	259	238
	100 bar O ₂ desiccated	341	250	244	238	242	239	246	214	251	243	226
	10 bar O ₂ desiccated	346	246	250	246	242	249	244	200	247	251	232
T-1f	10 bar Venus	303	217	213	203	204	204	202	192	204	206	211
	92 bar Venus	311	223	287	228	235	254	225	195	220	242	285
	1 bar H ₂ O	296	267	243	259	272	277	267	213	258	260	236
	1 bar H ₂ O cloudy	287	253	241	247	250	253	248	212	247	249	243
	10 bar CO ₂	277	201	260	200	221	235	200	172	185	206	263
	92 bar CO ₂	271	196	262	195	216	225	194	171	183	202	260
	100 bar O ₂ outgassing	229	209	218	219	202	234	208	192	221	224	222
T-1g	10 bar O ₂ outgassing	326	212	218	216	206	223	210	178	209	218	213
	100 bar O ₂ desiccated	268	225	228	216	210	209	219	192	227	213	194
	10 bar O ₂ desiccated	298	222	229	223	210	216	218	184	227	219	200
	10 bar Venus	272	189	210	188	193	193	188	171	184	189	199
	92 bar Venus	247	197	239	199	211	218	196	177	195	210	237
	10 bar CO ₂	231	181	236	180	203	205	179	160	170	185	232
	92 bar CO ₂	229	177	240	175	200	197	174	158	167	181	231
T-1h	100 bar O ₂ outgassing	209	191	199	199	188	202	192	180	205	204	194
	10 bar O ₂ outgassing	312	195	202	194	187	199	191	166	188	192	191
	100 bar O ₂ desiccated	224	207	210	200	192	187	201	180	208	189	176
	10 bar O ₂ desiccated	276	205	211	205	192	192	200	174	209	195	178
	10 bar Venus	242	173	210	173	183	181	173	158	168	174	190
	92 bar Venus	226	182	222	181	200	199	177	165	176	191	217
	10 bar CO ₂	174	157	217	155	176	167	154	145	150	157	186
T-1i	92 bar CO ₂	175	154	206	151	174	162	151	143	147	153	182
	100 bar O ₂ outgassing	195	168	171	170	166	169	167	163	174	172	164
	10 bar O ₂ outgassing	296	181	184	170	165	167	170	150	165	164	160
	100 bar O ₂ desiccated	199	183	185	179	170	161	177	165	181	162	149
	10 bar O ₂ desiccated	253	184	188	183	171	164	179	160	186	167	150
	10 bar Venus	209	155	185	153	162	161	153	145	149	154	162
	92 bar Venus	189	159	195	156	185	169	146	145	144	161	187

ORCID iDs

- Jacob Lustig-Yaeger <https://orcid.org/0000-0002-0746-1980>
 Victoria S. Meadows <https://orcid.org/0000-0002-1386-1710>
 Andrew P. Lincowski <https://orcid.org/0000-0003-0429-9487>

References

- Airapetian, V. S., Glocer, A., Khazanov, G. V., et al. 2017, *ApJL*, 836, L3
 Anglada-Escudé, G., Amado, P. J., Barnes, J., et al. 2016, *Natur*, 536, 437
 Arney, G., Domagal-Goldman, S. D., & Meadows, V. S. 2018, *AsBio*, 18, 311
 Arney, G. N., Meadows, V. S., Domagal-Goldman, S. D., et al. 2017, *AJ*, 836, 49
 Astropy Collaboration, Robitaille, T. P., Tollerud, E. J., et al. 2013, *A&A*, 558, A33
 Bagnasco, G., Kolm, M., Ferruit, P., et al. 2007, *Proc. SPIE*, 6692, 66920M
 Baraffe, I., Homeier, D., Allard, F., & Chabrier, G. 2015, *A&A*, 577, A42
 Barstow, J. K., Aigrain, S., Irwin, P. G. J., Kendrew, S., & Fletcher, L. N. 2016, *MNRAS*, 458, 2657
 Barstow, J. K., & Irwin, P. G. J. 2016, *MNRAS*, 461, L92
 Batalha, N., Stevenson, K., Hill, M., et al. 2018, Natashabatalha/PandExo: Starting PandExo Releases, Zenodo, doi:10.5281/zenodo.1256955
 Batalha, N. E., Lewis, N. K., Line, M. R., Valenti, J., & Stevenson, K. 2018, *ApJL*, 856, L34
 Batalha, N. E., Mandell, A., Pontoppidan, K., et al. 2017, *PASP*, 129, 064501
 Belu, A. R., Selsis, F., Morales, J.-C., et al. 2011, *A&A*, 525, A83
 Berta, Z. K., Charbonneau, D., Désert, J.-M., et al. 2012, *ApJ*, 747, 35
 Berta-Thompson, Z. K., Irwin, J., Charbonneau, D., et al. 2015, *Natur*, 527, 204
 Bétrémieux, Y., & Kaltenegger, L. 2014, *ApJ*, 791, 7
 Bétrémieux, Y., & Swain, M. R. 2018, *ApJ*, 865, 12
 Bolmont, E., Selsis, F., Owen, J. E., et al. 2017, *MNRAS*, 464, 3728
 Bouchet, P., García-Marín, M., Lagage, P.-O., et al. 2015, *PASP*, 127, 612
 Cowan, N. B., Agol, E., Meadows, V. S., et al. 2009, *ApJ*, 700, 915
 Cowan, N. B., Greene, T., Angerhausen, D., et al. 2015, *PASP*, 127, 311
 Csizmadia, S., Pasternacki, T., Dreyer, C., et al. 2013, *A&A*, 549, A9
 de Wit, J., Wakeford, H. R., Gillon, M., et al. 2016, *Natur*, 537, 69
 de Wit, J., Wakeford, H. R., Lewis, N. K., et al. 2018, *NatAs*, 2, 214
 Delrez, L., Gillon, M., Triaud, A. H. M. J., et al. 2018, *MNRAS*, 475, 3577
 Dittmann, J. A., Irwin, J. M., Charbonneau, D., et al. 2017, *Natur*, 544, 333
 Dong, C., Jin, M., Lingam, M., et al. 2018, *PNAS*, 115, 260
 Doyon, R., Hutchings, J. B., Beaulieu, M., et al. 2012, *Proc. SPIE*, 8442, 84422R
 Ehrenreich, D., Bonfils, X., Lovis, C., et al. 2014, *A&A*, 570, A89
 Feng, Y. K., Robinson, T. D., Fortney, J. J., et al. 2018, *AJ*, 155, 200
 Ferruit, P., Birkmann, S., Böker, T., et al. 2014, *Proc. SPIE*, 9143, 91430A
 Garcia-Sage, K., Glocer, A., Drake, J. J., Gronoff, G., & Cohen, O. 2017, *ApJL*, 844, L13
 Gillon, M., Jehin, E., Lederer, S. M., et al. 2016, *Natur*, 533, 221
 Gillon, M., Triaud, A. H. M. J., Demory, B.-O., et al. 2017, *Natur*, 542, 456
 Glasse, A., Rieke, G. H., Bauwens, E., et al. 2015, *PASP*, 127, 686
 Greene, T., Beichman, C., Eisenstein, D., et al. 2007, *Proc. SPIE*, 6693, 66930G
 Greene, T. P., Kelly, D. M., Stansberry, J., et al. 2017, *JATIS*, 3, 035001
 Greene, T. P., Line, M. R., Montero, C., et al. 2016, *ApJ*, 817, 17
 Grenfell, J. L., Grießmeier, J.-M., Patzer, B., et al. 2007, *AsBio*, 7, 208
 Grimm, S. L., Demory, B.-O., Gillon, M., et al. 2018, *A&A*, 613, A68
 Hedelt, P., von Paris, P., Godolt, M., et al. 2013, *A&A*, 553, A9
 Hu, R., Ehlmann, B. L., & Seager, S. 2012, *ApJ*, 752, 7
 Hunter, J. D. 2007, *CSE*, 9, 90
 Husser, T. O., Wende-von Berg, S., Dreizler, S., et al. 2013, *A&A*, 553, A6
 Kalirai, J. 2018, *ConPh*, 59, 251
 Kendrew, S., Scheithauer, S., Bouchet, P., et al. 2015, *PASP*, 127, 623
 Kirkland, L. E., Herr, K. C., & Adams, P. M. 2003, *JGRE*, 108, 5137
 Knutson, H. A., Benneke, B., Deming, D., & Homeier, D. 2014, *Natur*, 505, 66
 Kreidberg, L., Bean, J. L., Désert, J.-M., et al. 2014, *Natur*, 505, 69
 Kreidberg, L., & Loeb, A. 2016, *ApJL*, 832, L12
 Krissansen-Totton, J., Garland, R., Irwin, P., & Catling, D. C. 2018, *AJ*, 156, 114
 Liebert, J., & Gizis, J. E. 2006, *PASP*, 118, 659
 Lincowski, A., Lustig-Yaeger, J., & Meadows, V. 2019, *AJ*, 158, 26
 Lincowski, A. P., Meadows, V. S., Crisp, D., et al. 2018, *ApJ*, 867, 76
 Luger, R., & Barnes, R. 2015, *AsBio*, 15, 119
 Luger, R., Barnes, R., Lopez, E., et al. 2015, *AsBio*, 15, 57
 Luger, R., Lustig-Yaeger, J., & Agol, E. 2017a, *ApJ*, 851, 94
 Luger, R., Sestovic, M., Kruse, E., et al. 2017b, *NatAs*, 1, 0129
 Lustig-Yaeger, J., Meadows, V. S., Tovar Mendoza, G., et al. 2018, *AJ*, 156, 301
 Maurin, A. S., Selsis, F., Hersant, F., & Belu, A. 2012, *A&A*, 538, A95
 Meadows, V. S., Arney, G. N., Schwieerman, E. W., et al. 2018, *AsBio*, 18, 133
 Meadows, V. S., & Crisp, D. 1996, *JGR*, 101, 4595
 Miller-Ricci, E., Seager, S., & Sasselov, D. 2009, *ApJ*, 690, 1056
 Misra, A., Meadows, V., & Crisp, D. 2014, *ApJ*, 792, 61
 Moran, S. E., Hörst, S. M., Batalha, N. E., Lewis, N. K., & Wakeford, H. R. 2018, *AJ*, 156, 252
 Morley, C. V., Kreidberg, L., Rustamkulov, Z., Robinson, T., & Fortney, J. J. 2017, *ApJ*, 850, 121
 Morris, B. M., Agol, E., Davenport, J. R. A., & Hawley, S. L. 2018, *ApJ*, 857, 39
 Nicodemus, F. E. 1965, *ApOpt*, 4, 767
 Nikolov, N., Sing, D. K., Burrows, A. S., et al. 2015, *MNRAS*, 447, 463
 Peacock, S., Barman, T., Shkolnik, E. L., Hauschildt, P. H., & Baron, E. 2019, *ApJ*, 871, 235
 Pontoppidan, K. M., Pickering, T. E., Laidler, V. G., et al. 2016, *Proc. SPIE*, 9910, 991016
 Price-Whelan, A. M., Sipőcz, B. M., Günther, H. M., et al. 2018, *AJ*, 156, 123
 Rackham, B., Espinoza, N., Apai, D., et al. 2017, *ApJ*, 834, 151
 Rackham, B. V., Apai, D., & Giampapa, M. S. 2018, *ApJ*, 853, 122
 Robinson, T. D. 2017, *ApJ*, 836, 236
 Robinson, T. D. 2018, in Handbook of Exoplanets, ed. H. J. Deeg & J. A. Belmonte (Cham: Springer), 67
 Robinson, T. D., & Crisp, D. 2018, *JQSRT*, 211, 78
 Robinson, T. D., Meadows, V. S., & Crisp, D. 2010, *ApJL*, 721, L67
 Roettenbacher, R. M., & Kane, S. R. 2017, *ApJ*, 851, 77
 Rugheimer, S., Kaltenegger, L., Segura, A., Linsky, J., & Mohanty, S. 2015, *ApJ*, 809, 57
 Schaefer, L., Wordsworth, R. D., Berta-Thompson, Z., & Sasselov, D. 2016, *ApJ*, 829, 63
 Schlawin, E., Rieke, M., Leisenring, J., et al. 2017, *PASP*, 129, 015001
 Schwieerman, E. W., Kiang, N. Y., Parenteau, M. N., et al. 2018, *AsBio*, 18, 663
 Schwieerman, E. W., Meadows, V. S., Domagal-Goldman, S. D., et al. 2016, *ApJL*, 819, L13
 Segura, A., Kasting, J. F., Meadows, V., et al. 2005, *AsBio*, 5, 706
 Seinfeld, J., & Pandis, S. 2006, Atmospheric Chemistry and Physics (New York: Wiley)
 Selsis, F., Wordsworth, R. D., & Forget, F. 2011, *A&A*, 532, A1
 Sing, D. K., Fortney, J. J., Nikolov, N., et al. 2016, *Natur*, 529, 59
 STScI Development Team, 2013, Pysynphot: Synthetic Photometry Software Package, Astrophysics Source Code Library, ascl:1303.023
 van der Walt, S., Colbert, S. C., & Varoquaux, G. 2011, *CSE*, 13, 22
 Van Grootel, V., Fernandes, C. S., Gillon, M., et al. 2018, *ApJ*, 853, 30
 Vida, K., Kovářík, Z., Pál, A., Oláh, K., & Kriszkovics, L. 2017, *ApJ*, 841, 124
 Wang, S., Wu, D.-H., Barclay, T., & Laughlin, G. P. 2017, arXiv:1704.04290
 Weiss, L. M., & Marcy, G. W. 2014, *ApJL*, 783, L6
 Wordsworth, R. D., Schaefer, L. K., & Fischer, R. A. 2018, *AJ*, 155, 195
 Wunderlich, F., Godolt, M., Grenfell, J. L., et al. 2019, *A&A*, 624, A49
 Zhang, Z., Zhou, Y., Rackham, B. V., & Apai, D. 2018, *AJ*, 156, 178